The GEMstone

Volume 23, Issue 2 December 2013

Focus Group Final Reports

Table of Contents

GEMstone Newsletters are available online at:
http://aten.igpp.ucla.edu/gemwiki/index.php/Newsletters

The GEMstone Newsletter is edited by Peter Chi (gemeditor@igpp.ucla.edu) and Marjorie Sowmendran (margie@igpp.ucla.edu).

The distribution of GEMstone is supported by the National Science Foundation under Grant No. 0903107.

Dayside Field Aligned Current and Energy Deposition (FED) Focus Group (2010-2012): Final Report

Delores J. Knipp[1,2,*], Stefan Eriksson,[3] and Geoff Crowley[4]

The Dayside Field Aligned Current and Energy Deposition (FED) Focus Group (FG) commenced in 2010 to explain the relation between enhanced dayside field-aligned currents, their sources in the solar wind and their impacts in the ionosphere-thermosphere system. The FG's primary objective was to develop an understanding of the magnetospheric source of localized heating that produces unanticipated regions of dayside thermospheric expansion at high latitudes. A secondary objective was providing data-model comparison for events exhibiting this behavior. A tertiary objective was to improve GGCM specification of dayside energy input possibly associated with bowshock, dipole tilt (seasonal effects), and IMF B_X modulations. When the Focus Group was approved for a 2.5-year run instead of the requested 5-year run, the tertiary objective was dropped and the remaining research tasks were addressed with the following priority:

Priority 1 Strong IMF B_Y and precipitating particle effects

- Dayside energy sources and transport for events with large IMF B_Y (with B_Z +/-)
- Dayside field-aligned current systems for large in-the-ecliptic IMF (B_Y)
- The location and nature of Poynting and particle energy deposition for IMF B_Z>0
- The relation of such events to cusp region thermospheric neutral density anomalies
- Overall magnetospheric structure during large IMF B_Y disturbances
- Particle and conductivity influences on high-latitude heating events

Priority 2 Measurements and model-data comparison

- Methods for detecting such disturbances; indices vs. space-based monitors
- MHD modeling of such disturbances and model-data comparisons

Priority 3 Solar wind drivers, magnetospheric structure, asymmetry, seasonality

- The role of enhanced solar wind density and speed during such events
- Overall energy contributions to the coupled magnetosphere-ionosphere-thermosphere

Activities and Research Topics: **The Dayside FED FG inspired 16 peer-reviewed publications.** See list at the end. Researchers affiliated with the FED FG investigated magnetospheric disturbances that appeared to provide direct energy into the dayside thermosphere with little energy input to the magnetotail. The implication of such events is that the *Dst* index could remain unperturbed or even show storm recovery while the coupled dayside high-latitude region is greatly disturbed. This possibility was explored during the Joint GEM-CEDAR meeting in 2011. Results from the FED effort also linked to the M-I Coupling Ion Outflow FG and the GGCM Metrics FG. Additionally:

- At the first FED FG meeting a list of stor was proposed and posted on the GEM Wiki page. This list guided many of the subsequent model-data comparison stud-

1. Aerospace Engineering Sciences, University of Colorado Boulder, Colorado, USA
2. High Altitude Observatory, National Center for Atmospheric Research, Boulder, Colorado, USA
3. Laboratory for Atmospheric and Space Physics, University of Colorado, Boulder, Colorado USA (Co-organizer)
4. Atmospheric and Space Technology Research Associates LLC, Boulder, Colorado, USA (Co-organizer)

* Corresponding author
(E-mail: delores.knipp@colorado.edu)

ies.

- In addition to the summer and fall 2010, fall 2011 and summer 2012 GEM FED sessions at the GEM and Mini GEM meetings, the FED FG hosted a Joint GEM-CEDAR session during the 2011 joint meeting.

SUMMARY: *Carlson et al.* [2012] list four factors that cause the high-latitude cusp region to be sensitive to external energy input. 1) Strong velocity shears and flow channels near the cusp; 2) Strong vertical expansion over flow channels; Thermospheric density response to altitude dependent Joule heating; and 4) Thermospheric density response to altitude dependent electron density profile. FG activities investigated deeply items 1 and 4. Work on item 3 was underway as the FG ended.

Advances for Priority 1: Strong IMF B_Y and precipitating particle effects. The origin and influence of dayside strong, confined velocity shears and sunward flow channels during intervals of large IMF B_Y were amply demonstrated by: *Crowley et al.* [2010], *Knipp et al.* [2011], *Li et al.* [2011], *Eriksson and Rastätter* [2013] and *Wilder et al.* [2012a, 2012b and 2013]. Several of these studies showed IMF B_Z+ was also important in creating localized flow channels. The solar wind mechanical force and the $\mathbf{J} \times \mathbf{B}$ force act on the newly opened field high-latitude field lines created by cusp reconnection to produce a Pedersen current, which consequently generates an intense Joule heating region, and a pair of adjacent and opposite field-aligned currents (FACs) connecting to the magnetopause currents, forming a closed circuit. The intense Joule heating region is also the region with strong downward Poynting flux. The distribution, scale, and magnitude of this Joule heating region and corresponding FACs in the polar regions are mainly controlled by IMF clock angle, IMF magnitude, and solar wind dynamic pressure. A northward IMF condition with a large B_Y component will result in an extended region with intense Joule heating and FAC, thus making a spacecraft transiting the dayside region more likely to observe a strong downward Poynting flux. Convection in the flow channels and localized convection under northward IMF can lead to intense localized neutral upwelling, as well as large-scale gravity waves.

The role of soft particle precipitation in dayside energy deposition also came under scrutiny and debate. Both *Zhang et al.* [2012] and *Deng et al.* [2013] concluded that while soft electron precipitation have relatively minor effects on the interaction between the magnetosphere and ionosphere, they can significantly modify the plasma distribution of the F-region ionosphere and the neutral density of the thermosphere. Both papers attempted to quantify the interaction.

Advances for Priorities 2 and 3: Measurements, model-data comparison, solar wind drivers, magnetospheric structure and asymmetry, and seasonality. Easy access to CCMC runs-on-request was crucial to the success of the Dayside FED FG. The importance and necessity of satellite constellations (AMPERE and DMSP) for providing measurements and promoting model-data comparison cannot be overstated.

Outstanding Issues for Priority 1: The single most important aspect of unfinished FG business is the relative roles of Poynting flux and particle precipitation in the cusp region.

Outstanding Issues for Priorities 2 and 3: Even with the expanded data coverage provided by AMPERE and DMSP, several studies showed that the cusp region with confined regions of reverse convection were not covered with sufficient resolution to reveal important dynamics (see entries below). Further, numerous issues such as dynamic pressure effects; northern-southern hemisphere and day-night asymmetries and seasonal influences were not investigated adequately during the short FG lifetime.

DETAILS: Below are detailed outcomes from Priority 1, 2 and 3 tasks, as well as the Joint GEM-CEDAR discussions.

Outcomes from Priority 1 tasks: Strong IMF B_Y and precipitating particle effects. In all meetings of the FED FG there were active discussions of energy deposition and field aligned current structures related to events associated with large IMF B_Y and/or strong positive IMF B_Z.

Climatology:

To provide a background of FAC structure and orientation **Simon Wing** discussed source regions of dayside FAC based on statistical analysis of many years of DMSP data. *Wing et al.* [2011] found that each FAC sheet originates from more than one region in the magnetosphere, depending on the latitude and the magnetic local time. Region 0 FAC are located mostly on open field lines. Region1 FAC mostly map to closed field lines, in morning and afternoon, but near noon, they map mostly to the low latitude boundary layer. Region 2 FAC originate mostly from the central plasma sheet and boundary plasma sheet and and inner magnetosphere, all of which are on closed field lines. Near noon, some R2 may originate from the low-latitude boundary layer and can be on open or closed field lines.

Art Richmond showed statistical Poynting flux patterns from DE -2 derived from 18 months of data. The derived patterns show net Earth-directed Poynting flux. He showed that dayside energy deposition dominates for all IMF clock angles.

Delores Knipp presented patterns of extreme Poynting flux deposition associated with a large east-west interplanetary magnetic field component, based on DMSP data. *Knipp et al.* [2011] demonstrated that high-latitude Poynting flux was sometimes in excess of 100 mW/m^2—an order of magnitude above typical values. During intervals of large IMF B_Y the Poynting flux deposition peaks in the dayside with the pre/post noon maximum in Poynting flux depending on IMF B_Y sign. A significant fraction of these events occur with high-speed solar wind. The locations of these extreme events are consistent with the dayside flows channels discussed in *Li et al.* [2011].

Case and Event Studies:

Wenhui Li showed results from an OPENGGCM study of dayside energy deposition during northward IMF during the 21 Jan 2005 storm event. He was able to trace the field lines from the flank-merging region to the location of strong Poynting flux deposition shown in the DMSP data by *Knipp et al.* [2011]. *Li et al.* [2011] showed OPENGCM simulations for several events in late 2004 and in 2005. They conclude that flank merging is a source of FACs, dayside E x B flow channels and intense Poynting flux to the cusp.

Geoff Crowley provided an overview of thermospheric response from select events. *Crowley et al.* [2010] presented evidence of large thermospheric density effects associated with localized Poynting flux deposition based on CHAMP satellite data and simulations using the Thermosphere Ionosphere Mesosphere Electrodynamics General Circulation Model (TIMEGCM). The TIMEGCM was driven by high-fidelity high-latitude inputs specified by the Assimilative Mapping of Ionospheric Electrodynamics (AMIE) algorithm, and reproduced the main features of the density enhancements observed by CHAMP. This first detailed explanation of a high latitude density enhancement observed by CHAMP focused on the August 24, 2005 interval.

Stefan Eriksson reviewed Poynting flux observations for the 15 May 2005 storm: He showed the relation between high-latitude reconnection driven convection and NBZ currents and further illustrated FACs adjacent to well-defined flow channels. Subsequently he used DMSP and AMPERE magnetic perturbations for the 5 April 2010 storm to show IMF B_Y effects and dawnside FAC evolution during the early storm phase. This material is partially reported in a recent submission by *Wilder et al.* [2013]. Subsequently **Stefan Eriksson** described Alfvén Mach number and IMF clock angle dependencies of sunward directed ExB flow channels and their embedded Joule heating rates in the ionosphere. He showed a BATSRUS run from CCMC for 15 May 2005, highlighting field aligned currents and flow channels.

A BATSRUS simulation on the effects of Alfven Mach number and IMF clock angle on the location and flow speed magnitude within the magnetospheric counterparts of such flow channels is reported in *Eriksson and Rastätter* [2013].

Rick Wilder investigated intense Joule heating, thermospheric upwelling, and large-scale gravity waves and their association with reverse convection under northward IMF for April 5 2010. *Wilder et al.* [2012a] used AMPERE and AMIE data to show that reverse convection under northward IMF could also lead to intense localized upwelling, as well as large-scale gravity waves. During intervals of strong northward IMF there can be intense reverse convection that produces vertical winds and enhanced thermospheric density. Large-scale gravity waves with 700 m/s wave speed and 1000 km wavelength can arise from the density perturbations. The challenge for this event is separating solar wind dynamic pressure effects from IMF change effects. Subsequently *Wilder et al.* [2012b] used DMSP particle data and the AMIE convection patterns to show that the most intense cusp-region Joule heating occurred on streamlines which crossed the open-closed boundary. This confirmed the prediction by *Li et al.* [2011] that the intense energy deposition in the cusp on Aug 24, 2005 was driven by reconnection between the IMF and magnetosphere at high latitudes. Additionally, *Wilder et al.* showed that asymmetric reconnection theory [e.g. *Birn et al.*, 2008 and references therein] could be used to predict average ionospheric flow conditions in the channels where Joule heating was at its most intense.

Aaron Ridley: Investigated effects of concentrated dayside energy deposition on the global and regional thermosphere using a BATSRUS idealized simulation for 15 May 2005. He also reported neutral density enhancements associated with IMF BY and appropriately placed particle deposition.

Modeling:

Yue Deng showed the significance of different heating mechanisms to the cusp neutral density enhancement using the Global Ionosphere Thermosphere Model (GITM) nonhydrostatic model. She compared effectiveness of Poynting flux and soft particle precipitation in producing neutral density enhancements near the cusp. Using a specified input of Poynting flux of and soft electrons for a GITM simulation, *Deng et al.* [2013] showed that the Poynting flux increases the neutral density 34%. While the direct heating from soft electron precipitation (100 eV) produces only a 5% neutral density enhancement at 400 km, the associated enhanced ionization in the F-region from the electron precipitation leads to a neutral density enhancement of 24% through increased Joule heating. Thus, the net effect of the soft electron is close to 29% and the combined influence of Poynting flux and soft particle precipitation causes a more 50% increase in neutral density at 400 km, which is consistent with than CHAMP observations in extreme cases. The effect of electron precipitation on the neutral density at 400 km decreases sharply with increasing characteristic energy such that 900 eV electrons have little effect on neutral density. *Deng et al.,* [2013] conclude that the altitudinal distribution of energy input is important to neutral upwelling and TEC distribution and that soft particle deposition into the upper F region cusp is a very efficient heat source.

Brent Sadler (presented by **M. Lessard**): *Sadler et al.,* [2012] investigated soft electron precipitation effects at higher altitude using the Otto model. In the model auroral precipitation and Joule heating heat ambient electrons. The electron gas expands upward and the ions are pulled upward by the electric field. Ion momentum drags the neutrals upward. The estimated "cooking time" for this effect is 10-30 min: Electron temperatures rise in 1-3 min and upward ion velocity increases in 3-5 min. This should drive ion outflow and possibly enhanced neutral density structures in the F-region.

Binzheng Zhang discussed the roles of particles in heating the dayside near-cusp region. He used the coupled magnetosphere-ionosphere thermosphere model (LFM+TIEGCM = CMIT) to investigate the effects of precipitating soft electrons. *Zhang*

et al. [2012] included two types of soft electron precipitation - direct-entry cusp precipitation and Alfvén-wave induced, broadband electron precipitation - the effects of which were self-consistently included in a coupled global simulation model. Simulations show that while both types of soft electron precipitation have relatively minor effects on the interaction between the magnetosphere and ionosphere, they can significantly modify the plasma distribution of the F-region ionosphere and the neutral density of the thermosphere. Enhancements in F-region electron density and temperature and bottomside Pedersen conductivity caused by soft electron precipitation are shown to enhance the Joule heating per unit mass and the mass density of the thermosphere at F-region altitudes. The simulations provide a causal explanation of CHAMP satellite measurements of statistical enhancements in thermospheric mass density at 400 km altitudes in the cusp and pre-midnight auroral region.

Ramon Lopez suggested that some of the FAC associated with the large dayside energy deposition events originate at the bowshock during intervals of low Mach number [*Lopez et al.,* 2011].

Bob Strangeway discussed earlier work that related cusp-region FACs to IMF B_Y control and ion outflow using FAST data and. **Paul Song** discussed heating in the cusp region during northward IMF. **Betsy Mitchell** showed evidence from her Ph.D. dissertation that IMF B_Y decouples energy input into the ionosphere from energy input into the inner magnetosphere. This is the subject of a soon-to-be-submitted manuscript.

Outcomes from Priority 2 and 3 tasks: Measurements and model-data comparison and Solar wind drivers, magnetospheric structure and asymmetry, seasonality. In addition to the model data comparisons associated with task 1, the following investigations shed light on the relation between enhanced dayside field-aligned currents, their sources in the solar wind and their impacts in the ionosphere-thermosphere system.

Crowley et al. [2010] used TIMEGCM and AMIE to provide a global framework for interpretation of the CHAMP densities. These simulations revealed that the observed density enhancement in the dayside cusp region results from unexpectedly large amounts of energy entering the Ionosphere-Thermosphere system at cusp latitudes during an interval of strong (+20 nT) B_Y. The key data input in the AMIE runs was the DMSP data. When only magnetometers were ingested, the corresponding potential patterns were much smoother and the cross-cap potential was underestimated, and a thermospheric model driven by such AMIE patterns was unable to reproduce the Joule heating peak in the noon sector, and as a result failed to produce the observed density enhancement.

Gang Lu showed distributions of FACs and Poynting Flux under northward and southward IMF. She compared the individual satellite measurements with the global maps of Poynting flux derived from AMIE for November 2004 storm, and showed that even with 2 concurrent DMSP satellites (DMSP F-15 and F16), their coverage was not adequate to describe the full global energy storm deposition. She also showed dayside energy deposition during northward IMF and large east-west IMF. These results were reported in *Deng et al.* [2009].

Eric Lund presented sounding rocket measurements of electron heating in association with field-aligned currents and soft precipitation measured by the SCIFER rocket launch on 18 Jan 2008 over Svalbard. The rocket had an apogee of 1468 km. The rocket payload included a sensor that is designed to measure the temperature of thermal electrons. *Lund et al.* [2012] show that elevated electron temperatures measured in situ are correlated with electron precipitation as inferred from auroral emissions (poleward moving forms) during the 60–120 s preceding the passage of the rocket. This integrated "cooking time" is an important factor in determining the origin and resulting flux of outflowing ions.

Lasse Clausen showed global Poynting flux derived from SuperDARN and AMPERE measurements. He used SuperDARN and AMPERE to get 2-min average Poynting

flux. He showed example from 20 Dec 2010. He concluded that the AMPERE coverage may miss confined reverse-convection at high latitudes.

Slava Merkin used AMPERE, SuperDARN, and a Lyon-Fedder-Mobarry (LFM) global MHD simulation to deduce ionospheric electrodynamics. He reconstructed the potential distribution from AMPERE and compared this with SuperDARN. AMPERE and Super-DARN can help confirm conductances by rotations of flow vectors. The AMPERE data show NBZ system during August 3-4 2010 in the sunlit hemisphere. Using LFM, he mapped a Poynting flux patch in northern hemisphere to reconnection site in opposite hemisphere. Subsequently he compared (AMPERE) data and an ultra-high resolution (~60 km in the ionosphere) LFM simulation for an interval during the August 3-4 2010 storm, wherein there was a solar wind dynamic pressure jump and a south to north rotation of the IMF B_Z component with B_Y <0. The LFM and AMPERE current patterns showed remarkable agreement during this period. The dayside peak of the upward current moved from post-noon to pre-noon in response to the IMF B_Z rotation. He showed that the magnetic perturbations underlying AMPERE patterns were consistent with the simulated response. He also noted that, particularly during northward IMF conditions, if the orbit crossing point is far from the locus of the NBZ current system, the AMPERE fit may not capture the true geometry of the currents because the pole of the inversion basis functions is at the orbit crossing point rather than the magnetic pole. The new generation of AMPERE inversions fixes this problem by putting the basis function pole at the magnetic pole.

Delores Knipp showed dayside DMSP Poynting flux and soft particle asymmetries and compared those to CHAMP neutral enhancements. For all years and most conditions the enhancements were stronger in northern hemisphere cusp than in southern hemisphere cusp. As suggested by Art Richmond's climatology study in many instances the cusp energy deposition overwhelms the nightside energy deposition. Temporal variability of this effect is under investigation. She also showed dayside energy deposition for slow flow, high-speed streams and solar ejecta. High- speed streams compete with ejecta as the dominant dayside energy driver.

Outcomes from the Joint GEM-CEDAR 2011 Session. The joint GEM-CEDAR session supported a number of cross-disciplinary discussions that extended into investigations reported at the summer 2012 GEM meeting.

Herb Carlson showed 2-min resolution data from the EISCAT radar that likely contained Flux Transfer Events. (FTEs). The FTE's should pull solar-produced plasma into polar cap and create patches that give rise to polar cap scintillation. He suggested that poleward moving forms with signatures of particle flash are indicators of FTEs. *Carlson et al.* [2012] addressed four key aspects of cusp upwelling: 1) Ubiquitous strong velocity shears and flow channels near the cusp; 2) Strong vertical expansion over flow channels; Joule heating is a strong function of altitude; and 4) Thermospheric density response is strongly dependent on the electron density profile. Together these factors help explain the 10-50% cusp neutral density enhancements reported by *Luhr et al.* [2004].

Juan Rodriguez: Discussed auroral forms that extend equatorward from the persistent midday aurora during geomagnetically quiet periods. He showed data from a 630 nm allsky imager near the cusp. The auroral forms appeared equatorward of cusp near noon with east-west extent of 1000 km. These are possible flux transfer events. He also showed additional events called "crewcut" events. These are quiet-time auroral features extending equatorward from the dayside oval during negative *Bx* and B_Y-dominated conditions.

Chin Lin: Showed polar cap neutral density enhancements observed by the CHAMP accelerometer. He surveyed CHAMP neutral density data and searched for density perturbations that were two sigma or more above the previous 24-hour orbit average. He found a tendency for long lasting perturbations on dayside and near dawn. The

tendency appears to have strong IMF B_Y modulation. Further the high-latitude density peaks occur in summer hemisphere in 2001-2005.

Dan Weimer reviewed measurements and predictions of thermospheric temperature changes based on work he has done with drag data provided by US Space Command. He reported good global agreement from the empirical model.

Yi-Jiun Su discussed the high-altitude energy input to the thermospheric dynamics: for the August 4-7 2011 storm event. She compared density from DMSP and GRACE sensors, the High Accuracy Satellite Drag Model (HASDM), and the JB2008 and JB2008-with-Weimer-2005 models. She reported that the thermosphere responded immediately as the solar wind energy began to deposit energy into the high-latitude region; however, it took 6 hours to reach the maximum of the thermospheric energy. The thermosphere did not return to pre-storm level for a very long time. She estimated that the high latitude system transferred 3×10^{16} J of energy to 2.5×10^{16} J of heat—very efficient heat transfer.

Jiannan Tu: Discussed the time scales of dynamic Magnetosphere-Ionosphere -Thermosphere coupling. He characterized:

- Short time scale= Alfvén wave travel time
- Intermediate time scale = 10-20 min for quasi steady state
- Long time scale > 1 hr for steady state of entire M-I-T system

He reported most energy deposition is during intermediate time scales. *Tu et al.* [2011] investigated convection-driven ionosphere-thermosphere (I-T) heating using a three-fluid inductive approach. The M-I-T coupling was via a 1-D stratified atmosphere. They reported the heating to be essentially frictional in nature rather than Joule heating, as commonly assumed. The heating rate reaches a quasi-steady state after about 25 Alfvén travel times. Further, the dynamic heating rate can be more than twice greater than the quasisteady state value. The heating is strongest in the E-layer but the heating rate per unit mass is concentrated around the F-layer peak height. This implies a potential mechanism of driving O^+ upflow from O^+ rich F-layer. They also reported that the I-T heating caused by the magnetosphere-ionosphere coupling can be simply evaluated through the relative velocity between the plasma and neutrals without invoking field-aligned currents, ionospheric conductance, and electric field.

Athanasios Boudouridis presented a case study of the effect of solar wind dynamic pressure fronts on dayside field-aligned currents and thermospheric density for April 5 2010 using CHAMP data and TIMEGCM simulations. The challenge is to separate pressure pulse effects from IMF effects and determine their relative importance, since often both happen at same time. The pressure and IMF front passed ACE at ~ 0830 UT. The first responses were in the post-noon/afternoon MLT sector; these appear to coincide with intense FACs and Joule heating as produced in the AMIE procedure. The CHAMP and TIMEGCM results show enhanced neutral density in the same general region, but the magnitudes of the perturbations are not yet in agreement. The associated traveling atmospheric disturbance traveled to the equator in ~ 3.5 hr. More effort will be devoted to determining how common the response is and to determining the relative roles of the changing IMF and dynamic pressure.

Publications

Carlson, H. C., T. Spain, A. Aruliah, A. Skjaeveland, *and* J. Moen *(*2012*),* First-principles physics of cusp/polar cap thermospheric disturbances, Geophys. Res. Lett., 39, L19103, doi:10.1029/ 2012GL053034.

Crowley, G., D. J. Knipp, K. A. Drake, J. Lei, E. Sutton, *and* H. Lühr *(*2010*),* Thermospheric density enhancements in the dayside cusp region during strong BY conditions, *Geophys. Res. Lett., 37, L07110, doi:*10.1029/ 2009GL042143.

Deng. Y., T. Fuller-Rowell, A. J. Ridley, D. Knipp and R. Lopez, (2013) Theoretical study: influence of different energy

sources on the cusp neutral density enhancement, *J. Geophys. Res.* in press, DOI: 10.1002/jgra.50197.

Eriksson, S. and L. Rastätter (2013), Alfvén Mach number and IMF clock angle dependencies of sunward flow channels in the magnetosphere, *Geophys. Res. Lett., 40*, DOI: 10.1002/grl.50307.

Knipp, D., S. Eriksson, L. Kilcommons, G. Crowley, J. Lei, M. Hairston, *and* K. Drake *(*2011*),* Extreme Poynting flux in the dayside thermosphere: Examples and statistics, *Geophys. Res. Lett., 38,* L16102, doi:10.1029/2011GL048302.

Lopez, R. E., Merkin, V. G., and Lyon, J. G.: The role of the bow shock in solar wind-magnetosphere coupling, *Ann. Geophys., 29*, 1129-1135, doi:10.5194/angeo-29-1129-2011, 2011.

Lund, E. J., *et al. (*2012*),* Electron temperature in the cusp as measured with the SCIFER-2 sounding rocket, *J. Geophys. Res., 117,* A06326, doi:10.1029/2011JA017404.

Mitchell, E. J., R. E. Lopez, R. J. Bruntz, M. Wiltberger, J. G. Lyon, R. C. Allen, S. J. Cockrell, *and* P. L. Whittlesey *(*2010*),* Saturation of transpolar potential for large *Y* component interplanetary magnetic field, *J. Geophys. Res., 115,* A06201, *doi:*10.1029/2009JA015119.

Li, W., D. Knipp, J. Lei, *and* J. Raeder (2011), The relation between dayside local Poynting flux enhancement and cusp reconnection, *J. Geophys. Res., 116,* A08301, doi:10.1029/2011JA016566.

Sadler, F.B., et al., Auroral precipitation/ion upwelling as a driver of neutral density enhancement in the cusp. *Journal of Atmospheric and Solar-Terrestrial Physics* (2012), http://dx.doi.org/10.1016/j.jastp.2012.03.003.

Tu, J., P. Song, and V. M. Vasyliūnas (2011), Ionosphere/thermosphere heating determined from dynamic magnetosphere-ionosphere/thermosphere coupling, *J. Geophys. Res., 116,* A09311, doi:10.1029/2011JA016620.

Wilder, F. D., G. Crowley, B. J. Anderson, and A. D. Richmond (2012a), Intense dayside Joule heating during the 5 April 2010 geomagnetic storm recovery phase observed by AMIE and AMPERE, *J. Geophys. Res., 117*, A5, doi:10.1029/2012JA017547.

Wilder, F. D., G. Crowley, S. Eriksson, P. T. Newell, and M. R. Hairston (2012b), Ionospheric Joule heating, fast flow channels, and magnetic field line topology for IMF By-dominant conditions – Observations and comparisons with predicted reconnection jet speeds, *J. Geophys. Res.*, doi:10.1029/2012JA017914, in press.

Wilder, F. D., S. Eriksson, H. Korth, J. B. H. Baker, M. R. Hairston, C. Heinselman, and B. J. Anderson, Field-aligned current reconfiguration and magnetospheric response to an impulse in the interplanetary magnetic field (IMF) By Component, *Geophys. Res. Lett.*, submitted, 2013.

Wing, S., S. Ohtani, P. T. Newell, T. Higuchi, G. Ueno, *and* J. M. Weygand (2010), Dayside field-aligned current source regions, *J. Geophys. Res., 115,* A12215, doi:10.1029/2010JA015837.

Zhang, B., W. Lotko, O. Brambles, M. Wiltberger, W. Wang, P. Schmitt, *and* J. Lyon (2012), Enhancement of thermospheric mass density by soft electron precipitation, *Geophys. Res. Lett., 39,* L20102, doi:10.1029/2012GL053519.

Near-Earth Magnetosphere: Plasma, Fields, and Coupling Focus Group (2007-2012): Final Report

Sorin G. Zaharia,[1] Stanislav Sazykin,[2,*] and Benoit Lavraud[3]

Introduction

Throughout its lifetime (2007-2012), the GEM focus group "Near-Earth Magnetosphere: Plasma, Fields, and Coupling" served as a primary forum within the GEM structure for discussion and exchange of ideas regarding the physics of the inner magnetospheric plasmas (of ring current energies) and electromagnetic fields and connections of the inner magnetosphere to the plasma sheet and to the ionosphere. The focus group was proposed to the GEM Steering Committee in December 2006, and after its approval at the December meeting of the Steering Committee, it held its first sessions at the 2007 summer workshop. The focus group met every year at summer workshops and AGU (December) mini-workshops, with the final sessions held in 2012.

The group brought together inner magnetospheric modelers and experimentalists, facilitated discussions of unsolved questions, fostered cross-model comparisons, and provided floor for stimulating debates. The organizers wish to deem it a success, as a number of questions were answered, novel insights regarding the inner magnetosphere were obtained, new data sets were used to challenge the modelers, and common ground truth was established for a variety of first-principles models. These (but not all) achievements, which were facilitated (or at least the organizers hope so) by the existence of the focus group, are summarized briefly in the rest of this report.

The broad goals of the focus group were:

- To characterize large-scale electric and magnetic fields in the inner magnetosphere
- To understand how plasma sheet properties control the dynamics of the ring current
- To improve first-principles models of the inner magnetosphere by including physical self-consistency between the plasma and fields

The following **science questions** were targeted by the focus group:

- What are the effects of including self-consistent magnetic field in ring current models?
- What are the magnitudes of inductive electric fields in the inner magnetosphere?
- How do plasma sheet parameters and their cross-tail variations control ring current dynamics?
- What are the relative roles of various particle loss processes?
- How can convective electric field patterns be specified empirically in a more accurate fashion?

The list of **deliverables** expected at the conclusion of the focus group included:

- Modules (numerical models) for the inner magnetosphere with self-consistent fields and plasmas
- Empirical maps of convection electric

1. Los Alamos National Laboratory, Los Alamos, New Mexico, USA
2. School of Physics, Astronomy, and Computational Sciences, Rice University, Houston, Texas, USA
3. Institut de Recherche en Astrophysique et Planétologie, Université de Toulouse, Toulouse, France

* Corresponding author
(E-mail: sazykin@rice.edu)

fields
- Global maps of magnetic fields (modeled and empirical) for different geomagnetic conditions
- Understanding of the dependence of inner magnetospheric dynamics on plasma sheet properties

In what follows we briefly summarize some of the progress made to address these goals. Our emphasis is on surveying overall progress, with some examples illustrating major accomplishments. More details can be found in the publications cited and listed at the end.

Accomplishments

1. Development of Inner Magnetospheric Models.

The focus group commenced its activity shortly after the end of the GEM "Inner Magnetosphere/Storms" campaign. At the time, most inner magnetospheric models (some of them sometimes also called ring current models) did not have fully consistent electric and magnetic fields. These models underwent significant improvements during the lifetime of the focus group. In the first column of Table 1, we list some of the models that were discussed as part of the focus group work.

Major development of most of these numerical codes resulted in addition of new inputs, physics modules, or numerical methods. The 3rd, 4th, and 5th columns list the status of basic physics modules as of 2012 (information in Table 1 is supposed to be illustrative but not comprehensive).

2. Development of coupled models

In addition to standalone inner magnetospheric models (I/M), the focus group provided forum for discussion of and collaboration in development of coupled models of geospace that incorporated inner magnetosphere into global magnetospheric models. Table 2 lists several such examples, with reported additions and accomplishments listed in the rightmost column.

3. Empirical Field and Plasma Models

Empirical models of the inner magnetospheric electrostatic potential electric field [*Matsui et al.*, 2008; *Puhl-Quinn et al.*, 2008; *Matsui et al.*, 2010] were developed from Cluster data for use with ring current models that do not provide self-consistent electric field solutions [e.g., *Jordanova et al.*, 2009]. A standing challenge in designing such global characterization of convection is inclusion of subauroral polarization stream (SAPS) narrow flow channels and transient region-2 Birkeland currents shielding effects. SAPS electric fields structures are routinely observed with high-resolution HF radars [*Baker et al.*, 2007; *Greenwald et al.*, 2008; *Clausen et al.*, 2012].

Two recently developed empirical models of the magnetospheric magnetic field [*Tsyganenko and Sitnov*, 2007; *Kubyshkina et al.*, 2008; *Sitnov et al.*, 2008] were used by the modelers to provide data-based input for event simulations. Use of empirical dynamic models was proven to be an improvement over static magnetic field models [*Fok et al.*, 2010; *Ganushkina et al.*, 2010]; however, the morphology of the currents implied by empirical models is not always straightforward to interpret [*Sitnov et al.*, 2010].

Empirical models of the plasma sheet were also developed and analyzed that could be used to set boundary conditions on the nightside high-L boundaries of simulations [*Guild et al.*, 2008; *Lemon and O'Brien*, 2008; *Wang et al.*, 2009; *Wang et al.*, 2010; *Wang et al.*, 2011]. A way to estimate ion temperatures in the plasma sheet from ENA observations [*Keesee et al.*, 2011; *Keesee et al.*, 2012] provided an alternative way to specify ion temperature boundary condition for modeling the inner magnetosphere.

4. Understanding Inner Magnetospheric Dynamics

Self-consistent magnetic field

Modeling studies of idealized and real event simulations with codes that compute magnetic field self-consistent with the plas-

Table 1. Inner magnetospheric models used as part of the Near-Earth Magnetosphere (NEM) focus group work during 2007-2012.

Model/Institution	Modeling region (nightside)	E-field	B-field	Auroral Conductance	Development during lifetime of focus group
CRCM (GSFC) [*Buzulukova et al.*, 2010a; *Fok et al.*, 2010]	L<12	Self-consistent	Empirical	Empirical	Developed parallel version
RAM-SCB (LANL) [*Zaharia et al.*, 2008; *Jordanova et al.*, 2010; *Jordanova et al.*, 2012; *Yu et al.*, 2012]	L<10	Empirical	Self-consistent	N/A	Completed full coupling between kinetic ring current model and 3-D **B**-field equilibrium solver. Added induced **E**-fields
RCM (Rice) [*Yang et al.*, 2008; *Zhang et al.*, 2008; *Zhang et al.*, 2009a; *Zhang et al.*, 2009b]	L<25	Self-consistent	Empirical	Self-consistent	Addition of new empirical B-field models, plasma sheet boundary conditions.
RCM-E (Rice) [*Yang et al.*, 2011a; *Yang et al.*, 2012]	L<25	Self-consistent	Self-consistent	Self-consistent	Addition of MLT-varying outer plasma boundary condition
RCM (UCLA) [*Gkioulidou et al.*, 2009; *Gkioulidou et al.*, 2011; *Wang et al.*, 2011; *Gkioulidou et al.*, 2012]	L<25	Self-consistent	Self-consistent	Self-consistent	New data-based outer plasma boundary condition, self-consistent B-field
RCM-E (Aerospace) [*Chen et al.*, 2012]	L<10	Self-consistent	Self-consistent	Self-consistent	New numerical methods to solve for B-field consistently, addition of new plasma boundary condition.
HEIDI (UMich) [*Ilie et al.*, 2012a; *Ilie et al.*, 2012b]	L<6.6	Self-consistent or empirical	Arbitrary	Empirical	Reformulation for general B-field; addition of new models of geocorona for charge-exchange
IMPTAM UMich [*Ganushkina et al.*, 2012a; *Ganushkina et al.*, 2012b]	L<6.6	Empirical	Empirical	N/A	Addition of new event-based empirical B-field model

Table 2. Coupled geospace models with an inner magnetospheric module discussed during the lifetime of the focus group.

Model	Nature of coupling	Source	Achievements
RAM-SCB in SWMF	Global MHD drives I/M+self-consistent B-field	[*Zaharia et al.*, 2010]	Inclusion of ion composition in I/M improves model predictions.
RCM in SWMF	Global MHD with I/M, full coupling	[*Ganushkina et al.*, 2010; *Rastätter et al.*, 2013]	Better prediction of B-field at geo orbit.
CRCM in SWMF	Global MHD with I/M, full coupling	[*Buzulukova et al.*, 2010b; *Meng et al.*, 2012; *Glocer et al.*, 2013]	Full pitch-angle anisotropy in the ring current. Anisotropic MHD
LFM-RCM	Global MHD with I/M module, full coupling	[*Pembroke et al.*, 2012]	Prediction of entropy bubbles.
OpenGGCM with RCM	Global MHD with I/M, full coupling	[*Hu et al.*, 2010; *Hu et al.*, 2011]	Simulations suggest that entropy violation ("antidiffusion") precedes onset reconnection in substorms.

ma pressure [*Zaharia*, 2008; *Wu et al.*, 2009; *Gkioulidou et al.*, 2011; *Chen et al.*, 2012] showed conclusively that inclusion of a self-consistent magnetic field instead of a prescribed field leads to lower ion flux levels in the ring current and brings model predictions in closer agreement with observed values of ion fluxes [*Jordanova et al.*, 2010; *Gkioulidou et al.*, 2011; *Yang et al.*, 2011a; *Chen et al.*, 2012]. Furthermore, self-consistent magnetic field calculations are necessary to reproduce ground-based signatures of entropy channels used to approximate effects of the substorm expansion phase in the inner magnetosphere [*Yang et al.*, 2011b; *Yang et al.*, 2012].

Role of plasma sheet properties

Specification of the plasma sheet properties on the outer boundaries of inner magnetosphere models is another crucial physical input needed for ring current modeling. Simulations with several different models consistently show that:

- Formation of cold and dense plasma sheet following favorable geomagnetic conditions [*Lavraud and Jordanova*, 2007; *Guild et al.*, 2008; *Li et al.*, 2008] leads to the development of the ring current with its peak pressure higher in value and located closer to Earth [*Lavraud and Jordanova*, 2007; *Jordanova et al.*, 2009; *Jordanova et al.*, 2010; *Zheng et al.*, 2010; *Chen et al.*, 2012; *Jordanova et al.*, 2012].
- Allowing the properties of the plasma sheet to vary in MLT has a noticeable effect on the storm-time ring current [*Lavraud et al.*, 2008] allowing more efficient ring current injection in the post-

midnight sector. Furthermore, variations of the plasma moments in MLT were found necessary to model sawtooth oscillations [*Yang et al.*, 2008] and substorm-related particle injection [*Zhang et al.*, 2008; *Zhang et al.*, 2009a; *Zhang et al.*, 2009b].

Inductive electric fields

Zaharia et al. [2008] analyzed the role of induced electric fields, showing for a moderate storm that their role on ring current particle injection can be important at the peak of the main phase of a storm. A limitation of that study was the 1-hr interval for time changes – more recent work allowing 5 min. time steps for the B-field change show much stronger induced electric field effects at the peak, but also during the storm recovery phase. Aside from storms, [*Zhang et al.*, 2008; *Zhang et al.*, 2009b] found that in an isolated substorm, transport from the plasma sheet into the ring current is primarily due to the induced electric fields combined with gradient-curvature drifts. Thus, the role of inductive electric field can be important and depends on the type, phase and strength of geomagnetic activity.

Self-consistent electrodynamics

Simulations that include self-consistent electric field, Birkeland currents, and auroral precipitation were used to show that the ionospheric region of Harang discontinuity around midnight MLT can be explained in terms of differential gradient-curvature drifts and their role on formation of region-2 Birkeland currents [*Gkioulidou et al.*, 2009]. Another successful application of inner magnetospheric modeling with self-consistent electrodynamics was prediction of formation of SAPS channels and their time evolution in good agreement with Super-DARN HF-radar observations [*Clausen et al.*, 2012].

Role of loss processes

Relative roles of various loss processes in the ring current (charge exchange with geocorona, precipitation into the atmosphere due to pitch-angle scattering into the loss cone) were quantified to various degrees. In spite of recent progress, much remains to be learned about the magnitudes and time scales of these processes. While charge-exchange is a rather slow loss process for ring current particles, simulations of [*Ilie et al.*, 2012b] indicated that loss rates are sensitive to the assumed empirical models of geocorona. Another source of uncertainty is the assumed rate of precipitation of plasma sheet and ring current electrons and their control of auroral conductance [*Gkioulidou et al.*, 2012] and of higher-energy electrons that serve as the seed population for radiation belts [*MacDonald et al.*, 2008]. Furthermore, [*Siscoe et al.*, 2012] pointed out a seemingly MLT-dependent decay of the storm-time ring current unexplained by the existing theory or modeling. These results suggest that understanding of losses and their relative roles remains an open question.

Connections to other GEM FGs

The focus group collaborated with the GGCM Metrics and Validation (M&V) focus group in running a challenge that was part of the overall GEM 2008-2009 challenge and focused on the *Dst* prediction. Several inner magnetospheric models were run for the four selected storm intervals with various inputs, boundary conditions, and configurations. Results were archived in the CCMC online archive (http://ccmc.gsfc.nasa.gov/support/GEM_metrics_08/index.php), with initial overview of results published by [*Rastätter et al.*, 2013]. Some of the work related to loss of ring current particles due to precipitation due to wave-particle interaction was covered more extensively by the concurrent focus group "Diffuse Aurora".

Summary and Outlook

At its conclusion, the focus group has made significant contributions to all the science goals set in the beginning. As its legacy, it

leaves a number of inner magnetospheric models that received major improvements (both in terms of physics and numerical methods) from its developers. It also facilitated coupling several of these models with more global, MHD-based models of geospace.

References

Baker, J. B. H., R. A. Greenwald, J. M. Ruohoniemi, K. Oksavik, J. W. Gjerloev, L. J. Paxton, and M. R. Hairston (2007), Observations of ionospheric convection from the Wallops SuperDARN radar at middle latitudes, *J. Geophys. Res.*, *112*(1), A01303, doi:10.1029/2006ja011982.

Buzulukova, N., M. C. Fok, J. Goldstein, P. Valek, D. J. McComas, and P. C. Brandt (2010a), Ring current dynamics in moderate and strong storms: Comparative analysis of TWINS and IMAGE/HENA data with the Comprehensive Ring Current Model, *J. Geophys. Res.*, *115*(12), A12234, doi:10.1029/2010ja015292.

Buzulukova, N., M. C. Fok, A. Pulkkinen, M. Kuznetsova, T. E. Moore, A. Glocer, P. C. Brandt, G. Toth, and L. Rastatter (2010b), Dynamics of ring current and electric fields in the inner magnetosphere during disturbed periods: CRCM-BATS-R-US coupled model, *J. Geophys. Res.*, *115*, A05210, doi:10.1029/2009ja014621.

Chen, M. W., C. L. Lemon, T. B. Guild, M. Schulz, J. L. Roeder, and G. Le (2012), Comparison of self-consistent simulations with observed magnetic field and ion plasma parameters in the ring current during the 10 August 2000 magnetic storm, *J. Geophys. Res.*, *117*(A9), A09232, doi:10.1029/2012JA017788.

Clausen, L. B. N., J. B. H. Baker, J. M. Ruohoniemi, R. A. Greenwald, E. G. Thomas, S. G. Shepherd, E. R. Talaat, W. A. Bristow, Y. Zheng, A. J. Coster, and S. Sazykin (2012), Large-scale observations of a subauroral polarization stream by midlatitude SuperDARN radars: Instantaneous longitudinal velocity variations, *J. Geophys. Res.*, *117*(A5), A05306, doi:10.1029/2011ja017232.

Fok, M. C., N. Buzulukova, S. H. Chen, P. W. Valek, J. Goldstein, and D. J. McComas (2010), Simulation and TWINS observations of the 22 July 2009 storm, *J. Geophys. Res.*, *115*(12), A12231, doi:10.1029/2010ja015443.

Ganushkina, N. Y., M. W. Liemohn, M. V. Kubyshkina, R. Ilie, and H. J. Singer (2010), Distortions of the magnetic field by storm-time current systems in Earth's magnetosphere, *Ann. Geophys.*, *28*(1), 123-140, doi:10.5194/angeo-28-123-2010.

Ganushkina, N. Y., S. Dubyagin, M. Kubyshkina, M. Liemohn, and A. Runov (2012a), Inner magnetosphere currents during the CIR/HSS storm on July 21–23, 2009, *J. Geophys. Res.*, *117*, A00L04, doi:10.1029/2011ja017393.

Ganushkina, N. Y., M. W. Liemohn, and T. I. Pulkkinen (2012b), Storm-time ring current: model-dependent results, *Ann. Geophys.*, *30*(1), 177-202, doi:10.5194/angeo-30-177-2012.

Gkioulidou, M., C. P. Wang, L. R. Lyons, and R. A. Wolf (2009), Formation of the Harang reversal and its dependence on plasma sheet conditions: Rice convection model simulations, *J. Geophys. Res.*, *114*(7), A07204, doi:10.1029/2008ja013955.

Gkioulidou, M., C.-P. Wang, and L. R. Lyons (2011), Effect of self-consistent magnetic field on plasma sheet penetration to the inner magnetosphere: Rice convection model simulations combined with modified Dungey force-balanced magnetic field solver, *J. Geophys. Res.*, *116*(A12), A12213, doi:10.1029/2011ja016810.

Gkioulidou, M., C.-P. Wang, S. Wing, L. R. Lyons, R. A. Wolf, and T.-S. Hsu (2012), Effect of an MLT dependent electron loss rate on the magnetosphere-ionosphere coupling, *J. Geophys. Res.*, *117*(A11), doi:10.1029/2012ja018032.

Glocer, A., M. Fok, X. Meng, G. Toth, N. Buzulukova, S. Chen, and K. Lin (2013), CRCM + BATS-R-US Two Way Coupling, *J. Geophys. Res.*, n/a-n/a, doi:10.1002/jgra.50221.

Greenwald, R. A., K. Oksavik, R. Barnes, J. M. Ruohoniemi, J. Baker, and E. R. Talaat (2008), First radar measurements of ionospheric electric fields at sub-second temporal resolution, *Geophys. Res. Lett.*, *35*(3), L03111, doi:10.1029/2007gl032164.

Guild, T. B., H. E. Spence, E. L. Kepko, V. Merkin, J. G. Lyon, M. Wiltberger, and C. C. Goodrich (2008), Geotail and LFM comparisons of plasma sheet climatology: 1. average values, *J. Geophys. Res.*, *113*(4), A04216, doi:10.1029/2007ja012611.

Hu, B., F. R. Toffoletto, R. A. Wolf, S. Sazykin, J. Raeder, D. Larson, and A. Vapirev (2010), One-way coupled OpenGGCM/RCM simulation of the 23 March 2007 substorm event, *J. Geophys. Res., 115*, A12205, doi: 10.1029/2010ja015360.

Hu, B., R. A. Wolf, F. R. Toffoletto, J. Yang, and J. Raeder (2011), Consequences of violation of frozen-in-flux: Evidence from OpenGGCM simulations, *J. Geophys. Res.*, *116*(6), A06223, doi:10.1029/2011ja016667.

Ilie, R., M. W. Liemohn, G. Toth, and R. M. Skoug (2012a), Kinetic model of the inner magnetosphere with arbitrary magnetic field, *J. Geophys. Res.*, *117*(A4), A04208, doi:10.1029/2011ja017189.

Ilie, R., R. M. Skoug, H. O. Funsten, M. W. Liemohn, J. J. Bailey, and M. Gruntman (2012b), The impact of geocoronal density on ring current development, *J. Atmos. Sol.-Terr. Phys.*, doi:10.1016/j.jastp.2012.03.010.

Jordanova, V. K., H. Matsui, P. A. Puhl-Quinn, M. F. Thomsen, K. Mursula, and L. Holappa (2009), Ring current development during high speed streams, *J. Atmos. Sol.-Terr. Phys.*, *71*(10-11), 1093-1102, doi:10.1016/j.jastp.2008.09.043.

Jordanova, V. K., S. Zaharia, and D. T. Welling (2010), Comparative study of ring current development using empirical, dipolar, and self-consistent magnetic field simulations, *J. Geophys. Res.*, *115*, A00J11, doi:10.1029/2010ja015671.

Jordanova, V. K., D. T. Welling, S. G. Zaharia, L. Chen, and R. M. Thorne (2012), Modeling ring current ion and electron dynamics and plasma instabilities during a high-speed stream driven storm, *J. Geophys. Res.*, *117*, A00L08, doi:10.1029/2011ja017433.

Keesee, A. M., N. Buzulukova, J. Goldstein, D. J. McComas, E. E. Scime, H. Spence, M. C. Fok, and K. Tallaksen (2011), Remote observations of ion temperatures in the quiet time magnetosphere, *Geophys. Res. Lett.*, *38*(3), L03104, doi:10.1029/2010gl045987.

Keesee, A. M., J. G. Elfritz, D. J. McComas, and E. E. Scime (2012), Inner magnetosphere convection and magnetotail structure of hot ions imaged by ENA during a HSS-driven storm, *J. Geophys. Res.*, *117*(5), A00l06, doi:10.1029/2011ja017319.

Kubyshkina, M., T. I. Pulkkinen, N. Y. Ganushkina, and N. Partamies (2008), Magnetospheric currents during sawtooth events: Event-oriented magnetic field model analysis, *J. Geophys. Res.*, *113*(A8), doi:10.1029/2007ja012983.

Lavraud, B., and V. K. Jordanova (2007), Modeling the effects of cold-dense and hot-tenuous plasma sheet on proton ring current energy and peak location, *Geophys. Res. Lett.*, *34*(2), L02102, doi:10.1029/2006GL027566.

Lavraud, B., V. K. Jordanova, and M. F. Thomsen (2008), Modeling the effects of local time variation of plasma sheet properties on proton ring current energy and peak location, *J. Geophys. Res.*, *113*(5), A05215, doi:10.1029/2007JA012883.

Lemon, C. L., and T. P. O'Brien (2008), A solar wind driven model of geosynchronous plasma moments, *Adv. Space Res.*, *41*(8), 1226-1233, doi:10.1016/j.asr.2007.08.028.

Li, W., J. Raeder, M. F. Thomsen, and B. Lavraud (2008), Solar wind plasma entry into the magnetosphere under northward IMF conditions, *J. Geophys. Res.*, *113*(4), A04204, doi:10.1029/2007ja012604.

MacDonald, E. A., M. H. Denton, M. F.

Thomsen, and S. P. Gary (2008), Superposed epoch analysis of a whistler instability criterion at geosynchronous orbit during geomagnetic storms, *J. Atmos. Sol.-Terr. Phys.*, *70*(14), 1789-1796, doi:10.1016/j.jastp.2008.03.021.

Matsui, H., P. A. Puhl-Quinn, V. K. Jordanova, Y. Khotyaintsev, P. A. Lindquist, and R. B. Torbert (2008), Derivation of inner magnetospheric electric field (UNH-IMEF) model using Cluster data set, *Ann. Geophys.*, *26*, 2887-2898, doi:10.5194/ angeo-26-2887-2008.

Matsui, H., P. A. Puhl-Quinn, J. W. Bonnell, C. J. Farrugia, V. K. Jordanova, Y. V. Khotyaintsev, P. A. Lindqvist, E. Georgescu, and R. B. Torbert (2010), Characteristics of storm time electric fields in the inner magnetosphere derived from Cluster data, *J. Geophys. Res.*, *115*, A11215, doi:10.1029/2010ja015450.

Meng, X., G. Tóth, M. W. Liemohn, T. I. Gombosi, and A. Runov (2012), Pressure anisotropy in global magnetospheric simulations: A magnetohydrodynamics model, *J. Geophys. Res.*, *117*(8), A08216, doi:10.1029/2012ja017791.

Pembroke, A., F. Toffoletto, S. Sazykin, M. Wiltberger, J. Lyon, V. Merkin, and P. Schmitt (2012), Initial results from a dynamic coupled magnetosphere-ionosphere-ring current model, *J. Geophys. Res.*, *117*(A2), A02211, doi:10.1029/2011ja016979.

Puhl-Quinn, P. A., H. Matsui, V. K. Jordanova, Y. Khotyaintsev, and P. A. Lindqvist (2008), An effort to derive an empirically based, inner-magnetospheric electric field model: Merging Cluster EDI and EFW data, *J. Atmos. Sol.-Terr. Phys.*, *70*(2-4), 564-573, doi:10.1016/j.jastp.2007.08.069.

Rastätter, L., M. M. Kuznetsova, A. Glocer, D. Welling, X. Meng, J. Raeder, M. Wiltberger, V. K. Jordanova, Y. Yu, S. Zaharia, R. S. Weigel, S. Sazykin, R. Boynton, H. Wei, V. Eccles, W. Horton, M. L. Mays, and J. Gannon (2013), Geospace environment modeling 2008–2009 challenge: Dst index, *Space Weather*, *11*(4), 187-205, doi:10.1002/swe.20036.

Siscoe, G. L., J. J. Love, and J. L. Gannon (2012), Problem of the Love-Gannon relation between the asymmetric disturbance field and Dst, *J. Geophys. Res.*, *117*(9), doi:10.1029/2009sw000518.

Sitnov, M. I., N. A. Tsyganenko, A. Y. Ukhorskiy, and P. C. Brandt (2008), Dynamical data-based modeling of the storm-time geomagnetic field with enhanced spatial resolution, *J. Geophys. Res.*, *113*(7), A07218, doi:10.1029/2007ja013003.

Sitnov, M. I., N. A. Tsyganenko, A. Y. Ukhorskiy, B. J. Anderson, H. Korth, A. T. Y. Lui, and P. C. Brandt (2010), Empirical modeling of a CIR-driven magnetic storm, *J. Geophys. Res.*, *115*, doi:10.1029/ 2009ja015169.

Tsyganenko, N. A., and M. I. Sitnov (2007), Magnetospheric configurations from a high-resolution data-based magnetic field model, *J. Geophys. Res.*, *112*(A6), A06225, doi:10.1029/2007ja012260.

Wang, C. P., L. R. Lyons, R. A. Wolf, T. Nagai, J. M. Weygand, and A. T. Y. Lui (2009), Plasma sheet Pv5/3and nv and associated plasma and energy transport for different convection strengths and AE levels, *J. Geophys. Res.*, *114*(4), A00D02, doi:10.1029/2008JA013849.

Wang, C. P., L. R. Lyons, T. Nagai, J. M. Weygand, and A. T. Y. Lui (2010), Evolution of plasma sheet particle content under different interplanetary magnetic field conditions, *J. Geophys. Res.*, *115*, A06210, doi:10.1029/2009ja015028.

Wang, C. P., M. Gkioulidou, L. R. Lyons, R. A. Wolf, V. Angelopoulos, T. Nagai, J. M. Weygand, and A. T. Y. Lui (2011), Spatial distributions of ions and electrons from the plasma sheet to the inner magnetosphere: Comparisons between THEMIS-Geotail statistical results and the Rice convection model, *J. Geophys. Res.*, *116*(11), A11216, doi:10.1029/2011ja016809.

Wu, L., F. Toffoletto, R. A. Wolf, and C. Lemon (2009), Computing magnetospheric equilibria with anisotropic pressures, *J.*

Geophys. Res., *114*(A5), A05213, doi:10.1029/2008ja013556.

Yang, J., F. R. Toffoletto, R. A. Wolf, S. Sazykin, R. W. Spiro, P. C. Brandt, M. G. Henderson, and H. U. Frey (2008), Rice Convection Model simulation of the 18 April 2002 sawtooth event and evidence for interchange instability, *J. Geophys. Res., 113*(A11), A11214, doi: 10.1029/2008ja013635.

Yang, J., F. R. Toffoletto, R. A. Wolf, and S. Sazykin (2011a), RCM-E simulation of ion acceleration during an idealized plasma sheet bubble injection, *J. Geophys. Res.*, *116*(A5), A05207, doi:10.1029/2010ja016346.

Yang, J., R. A. Wolf, and F. R. Toffoletto (2011b), Accelerated thinning of the near-Earth plasma sheet caused by a bubble-blob pair, *Geophys. Res. Lett.*, *38*(1), L01107, doi:10.1029/2010gl045993.

Yang, J., F. R. Toffoletto, R. A. Wolf, S. Sazykin, P. A. Ontiveros, and J. M. Weygand (2012), Large-scale current systems and ground magnetic disturbance during deep substorm injections, *J. Geophys. Res.*, *117*(A4), A04223, doi:10.1029/2011ja017415.

Yu, Y., V. Jordanova, S. Zaharia, J. Koller, J. Zhang, and L. M. Kistler (2012), Validation study of the magnetically self-consistent inner magnetosphere model RAM-SCB, *J. Geophys. Res.*, *117*(3), A03222, doi:10.1029/2011JA017321.

Zaharia, S. (2008), Improved Euler potential method for three-dimensional magnetospheric equilibrium, *J. Geophys. Res.*, *113*(A08221).

Zaharia, S., V. K. Jordanova, M. F. Thomsen, and G. D. Reeves (2008), Self-consistent geomagnetic storm simulation: The role of the induced electric fields, *J. Atmos. Sol.-Terr. Phys.*, *70*(2-4), 511-518, doi:10.1016/j.jastp.2007.08.067.

Zaharia, S., V. K. Jordanova, D. Welling, and G. Toth (2010), Self-consistent inner magnetosphere simulation driven by a global MHD model, *J. Geophys. Res.*, *115*, A12228, doi:10.1029/2010ja015915.

Zhang, J. C., R. A. Wolf, S. Sazykin, and F. R. Toffoletto (2008), Injection of a bubble into the inner magnetosphere, *Geophys. Res. Lett., 35*(2), L02110, doi: 10.1029/2007gl032048.

Zhang, J. C., R. A. Wolf, G. M. Erickson, R. W. Spiro, F. R. Toffoletto, and J. Yang (2009a), Rice Convection Model simulation of the substorm-associated injection of an observed bubble into the inner magnetosphere: 1. Magnetic field and other inputs, *J. Geophys. Res.*, *114*, A08218, doi:10.1029/2009ja014130.

Zhang, J. C., R. A. Wolf, R. W. Spiro, G. M. Erickson, S. Sazykin, F. R. Toffoletto, and J. Yang (2009b), Rice Convection Model simulation of the substorm-associated injection of an observed plasma bubble into the inner magnetosphere: 2. Simulation results, *J. Geophys. Res., 114*, A08219, doi: 10.1029/2009ja014131.

Zheng, Y. H., A. T. Y. Lui, and M. C. Fok (2010), Effects of plasma sheet properties on storm-time ring current, *J. Geophys. Res.*, *115*, A08220, doi:10.1029/2009ja014806.

Plasma Entry and Transport into and within the magnetotail (PET) Focus Group (2008-2012): Final Report

Simon Wing[1], Jay R. Johnson[2] , and Antonius Otto[3]

Abstract. The GEM Plasma Entry and Transport into and within the magnetotail (PET) focus group's goal was to improve understanding of the magnetotail—how it is populated and how plasma is redistributed by physical processes that occur in the magnetotail. The plasma sheet is primarily populated by the solar wind. Three solar entry mechanisms are examined: (1) double cusp reconnection [*Song and Russell*, 1992], (2) KHI [e.g., *Otto and Fairfield*, 200], and (3) KAW [*Johnson and Cheng*, 1997]. These three mechanism have been shown to be effective at transporting solar wind particles into the magnetotail during northward IMF, although KHI and KAW can also operate at other IMF orientations. All three mechanisms can efficiently fill the plasma sheet with cold dense ions during northward IMF. However, the double cusp reconnection entry rate is proportional to $\sim n_{sh}^{0.5}$ whereas KAW and KHI entry rate is proportional to $\sim n_{sh}$. Observations of the dawn-dusk density and temperature asymmetries suggest that KAW may be important in heating particles at the dawn flank magnetopause. Solar wind entrees lower the specific entropy ($s=p/\rho^{\gamma}$) along the flanks. Temperatures and specific entropies increase when the solar wind particles are transported across the magnetopause, but ion-to-electron temperature ratio is roughly conserved. The plasma sheet may also be populated by ionospheric outflows that result from transverse ion heating, Alfven Poynting fluxes, wave-particle interactions associated with field-aligned currents, centrifugal acceleration, ambipolar outflows associated with photoionization of electrons. Within the plasma sheet, transport is primarily controlled by the direction of the IMF leading to a relatively cold, dense, stagnant population during northward IMF conditions with relatively slow inward transport towards the center of the plasma sheet. During southward IMF conditions transport is dominated by intermittent periods of fast magnetospheric convection such as fast flows and dipolarizations associated with substorms. Turbulence is a common property in the mid- to far-tail and tends to dominate transport processes in those regions. Transport within the plasma sheet has been described with MHD models, which conserve entropy. Total entropy (pV^{γ}) conservation provides important constraints on the accessibility of plasma to the plasma sheet and governs the redistribution of plasma when flux tubes are depleted of total entropy due to nonadiabatic processes such as reconnection, plasma diffusion, and wave-particle interactions. The PET focus group used the framework of entropy to examine plasma entry, magnetotail transport, fast flows, and magnetotail state transitions associated with substorms. Finally, the PET focus group also included discussion of comparative magnetotails, such as Jupiter and Saturn, considering similarities and differences with Earth's magnetosphere.

Keywords: solar wind entry, ion outflows, particle transport, reconnection, Kelvin-

1. Applied Physics Laboratory, The Johns Hopkins University, Laurel, Maryland, USA
2. Princeton Plasma Physics Laboratory, Princeton, New Jersey, USA
3. Geophysical Institute University of Alaska, Fairbanks, Alaska, USA

* Corresponding author
(E-mail: Simon.Wing@jhuapl.edu)

Helmholtz, Kinetic Alfven wave (KAW), entropy, fast flow, turbulence, ion to electron temperature ratio.

1. Introduction

The Earth's magnetosphere on the nightside is stretched out in an elongated fashion that resembles a tail like configuration, which is often referred to as magnetotail. The magnetotail is fundamentally important for understanding dynamical processes in the magnetosphere such as geomagnetic storms and substorms. A region in the magnetotail that is usually characterized by high plasma density (n > 0.5 cm^{-3}) and high plasma b is called the plasma sheet, which is an important source population for ring current, energetic outer radiation belt particles, and auroral precipitation.

It is believed that there are only two plasma sources for the plasma sheet namely, the solar wind and the ionosphere. Their relative importance depends on solar wind and geomagnetic conditions.

It has been argued based on observations that the ionosphere is a fully adequate source to populate the magnetosphere [*Chappell*, 1987]. **Welling** [PET, 2009] showed global simulations in which the ionosphere was the primary source of the plasma sheet for southward IMF, while the solar wind was the primary source for northward IMF.

On the other hand, it is well established that plasma sheet properties such as density, pressure, and temperature are correlated with solar wind conditions [e.g., *Borovsky et al.,* 1998a; *Terasawa et al.,* 1997; *Wing and Newell*, 2002; *Nagata et al.,* 2008]. For example, **Wang** [PET, 2006] reported that higher solar wind velocity increases plasma sheet temperature and higher solar wind density increases plasma sheet density. Plasma sheet energetic electrons are correlated with solar wind velocity, but not solar wind energetic electrons or IMF [*Burin des Roziers et al.,* 2009; **X. Li**, PET, 2008]. **Yiqun Yu** [PET, 2007] showed that plasma sheet thermal pressure correlates with solar wind *Vx*, but not dynamic pressure. However, the path the solar wind takes to reach the plasma sheet and the plasma transport within the plasma sheet are still a major unresolved question in space physics.

During southward Interplanetary Magnetic Field (IMF), reconnection can occur at the low latitude magnetopause on the dayside where the IMF and the Earth's magnetic field line are nearly anti-parallel [*Crooker*, 1979]. After reconnection, the open field lines would convect to the nightside toward the lobe region. Because of the solar wind duskward electric field, these open field lines would ExB drift to the equatorial region where they would once again reconnect [e.g. *Pedersen et al.,* 1985]. This process is depicted in Figure 1. Once reconnected, the field line, which is filled with magnetosheath plasma, becomes part of the plasma sheet. In essence, the magnetosheath plasma is now captured in the plasma sheet. Subsequently, this newly closed field line would ExB convect sunward to the dayside, returning the magnetic flux back to the dayside. This process is known as the Dungey cycle [*Dungey*, 1961], although the solar wind entry into the plasma sheet during southward IMF can be more complicated than the Dungey cycle and can involve other processes.

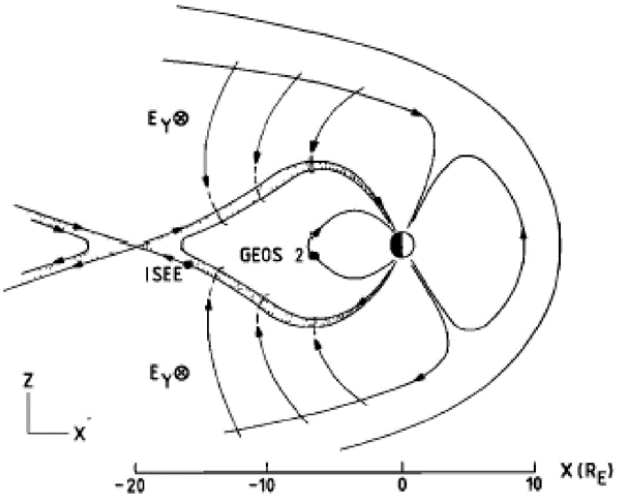

Figure 1. (from Figure 11 of *Pedersen et al.* [1985])

In the anti-parallel merging model [*Crooker*, 1979], the reconnection would occur at high-latitude poleward of the cusp in the lobe during northward IMF. After the reconnection, the footpoint of the newly reconnected field line would initially move sunward before being swept away to the nightside, but the solar wind electric field is dawnward, instead of duskward for southward IMF case. So, the entry mechanism for northward IMF would not be as simple and straightforward as the scenario portrayed in the Dungey cycle. The intrigue and the difficulty only deepened when it was discovered that compared to southward IMF conditions, more solar wind particles enter the magnetotail during northward IMF conditions, which can lead to the formation of cold, dense plasma sheet [e.g., *Terasawa et al.,* 1997; *Fujimoto et al.*, 1998; *Wing and Newell*, 2002; *Stenuit et al.,* 2002].

It turns out, reconnection can still play an important role in transporting solar wind plasma into the magnetotail during periods of northward IMF. A special case of high latitude reconnection, where the Earth's field lines are reconnected at both hemispheres, forming a newly closed field line filled with magnetosheath plasma [*Song and Russell*, 1992; *Le et al.,* 1996; *Sandholt et al.,* 1999; *Fuselier et al.,* 2002]. Magnetohydrodynamic (MHD) simulations have been performed to show that this process can effectively bring magnetosheath plasma into plasma sheet [*Raeder et al.,* 1995; 1997; PET, 2009]. This process is depicted in Figure 2, which shows the time sequence of the newly field line from the time of reconnection to the convection to the magnetotail flank in an MHD simulation [*Li et al.,* 2005; PET, 2007]. Initially, the newly closed dayside field line would move sunward and then it would move tailward to the flanks. In MHD simulations, this whole process can take about 90 min [*Li et al.,* 2008]. *Øieroset et al.* [2005] reported a fairly good agreement in temperature and density between an MHD simulation and Cluster satellite observations in a case study. MHD simulations for northward IMF conditions replicate the development of a low-latitude boundary layer detected by the five THEMIS spacecraft as they encountered the magnetopause boundary [*Li et al.,* 2009].

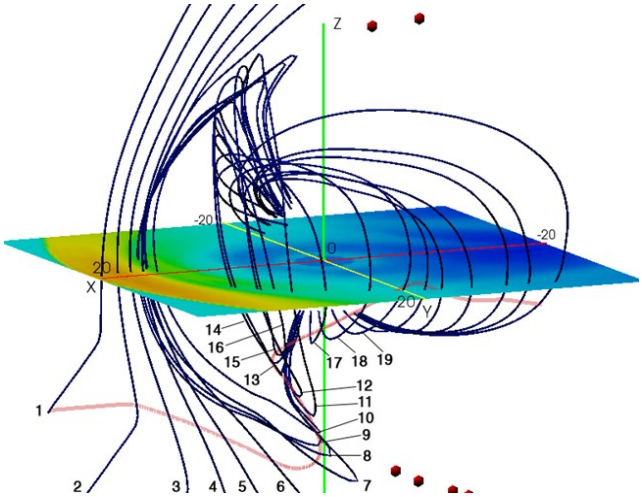

Figure 2. (from *Li et al.* [2005])

Another possible solar wind entry mechanism is Kelvin-Helmholtz Instability (KHI). Kelvin-Helmholtz waves grow along an inhomogeneous velocity shear layer (as found on the flank magnetopause) and eventually develop a rolled up vortex pattern in density and magnetic field, as illustrated in Figure 3. KHI has been successfully simulated with MHD code [e.g., *Otto and Fairfield*, 2000; *Nakamura and Fujimoto*, 2005; *Nykyri and Otto*, 2001; *Nykyri et al.,* 2006; *Guo et al.,* 2010]. Signatures of these vortices have been found on the dusk and dawn flanks of the magnetosphere [e.g., *Fairfield et al.,* 2000; *Fujimoto et al.,* 2003; *Hasegawa et al.,* 2006]. KHI periodically compresses the magnetopause current sheet, setting up conditions for reconnection to occur [**Otto**, PET, 2006]. Moreover, reconnection in the nonlinear stage of the K-H instability could lead to the detachment of plasma from the vortex structures, leading to significant magnetopause transport [e.g., *Otto and Fairfield,* 2000; *Nykyri et al.,* 2006]. Hybrid simulations have indicated that ion blobs could become detached from the vortex structure of the K-H instability and could provide filaments, producing a mixing of plasma in the shear layer [*Thomas and Winske*, 1991; 1993; *Fu-*

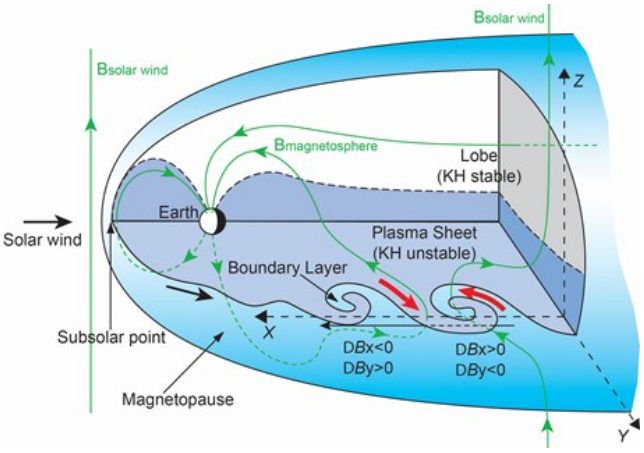

Figure 3. (from *Hasegawa et al.* [2004b])

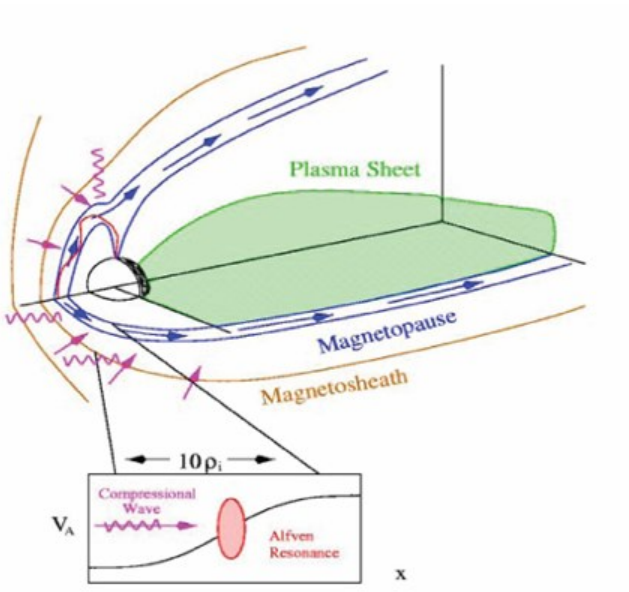

Figure 4. (**Johnson**, PET, 2010)

jimoto and Terasawa, 1994; 1995]. *Hasegawa et al.* [2006] has developed criteria for detecting rolled up KH vortices with a single spacecraft that can be implemented as an automated computer algorithm.

Large-amplitude Alfvén waves have also been observed on the magnetospheric boundary [e.g., *Tsurutani et al.,* 1982; LaBelle and Treumann, 1988; Anderson and Fuselier, 1994]. There is evidence that the waves could be the result of mode conversion of magnetosheath compressions in the sharp magnetopause gradients at the magnetopause [*Lee et al.,* 1994; *Johnson and Cheng*, 1997; *Johnson et al.,* 2001]. Because the wavelength of the mode converted waves are on the order of the ion gyroradius, they can lead to efficient convective and diffusive transport of ions across the magnetopause, as illustrated in Figure 4 [*Johnson and Cheng,* 1997; *Chen*, 1999; *Chaston et al.,* 2008]. The mode conversion process has been simulated with 2D hybrid simulations [*Lin et al.,* 2010] showing linear mode conversion, and 3D simulations [*Lin et al.,* 2012] showing nonlinear decay of the mode converted waves such that transport is greatly enhanced because of the development of modes with large azimuthal wave number.

These three processes are not necessarily mutually exclusive and have all been demonstrated to be capable to transport plasma across magnetic boundaries. For example, KH waves can excite KAW [*Sibeck et al.,* 1999]. KAWs have been observed in conjunction with reconnection and Kelvin-Helmholtz structures [*Chaston et al.,* 2005, 2007, 2009] and [PET, 2007]. *Nishino et al.* [2007] also observed bidirectional electrons and cold protons inside a KH vortical structure, which they interpreted as a signature of reconnection. Additionally, they observed electron and ion heating, which they attributed to wave-particle interactions such as KAW heating [*Johnson and Cheng*, 1997]. Taylor and *Lavraud* [2008] found that there could be three distinct ion populations, which can be interpreted as evidence for KAW, KHI, and reconnection processes. KHI and KAW can also play significant roles in the plasma entry during southward IMF. **Nykyri** [PET, 2009] also presented three component ions with similar interpretation.

It has been a challenge to distinguish which of these three mechanisms can play a more significant role and under what conditions. Recent observations have attempted to identify several potential discriminators based on both in situ and remote sensing methods. One of the potential discriminators is the filling rate. Each entry mechanism may lead to a different entry or filling rate. Another potential discriminator is the dawn-dusk asymmetries. Dawn-dusk asymmetries

are particularly interesting because they may be related to how upstream boundary conditions (e.g. Parker spiral magnetic field orientation) affect the various entry mechanisms, which can be tested by observation and theory. Another potential discriminator is the specific entropy or entropy per unit volume (p/n^{γ} where γ is polytropic index). Changes in the entropy profiles may be indicators that nonadiabatic processes are operating in conjunction with plasma transport, and how the entropy changes is likely related to the entry mechanism.

While cold plasma is preferentially observed in the plasma sheet during periods of northward IMF, hot plasma is preferentially observed during periods of southward IMF. However, both hot and cold plasma have been observed to co-exist in the same region/field-line under all IMF conditions. The mechanism for heating cold plasma, either solar wind or ionospheric origin, to hot plasma population has not been firmly established, but it does appear that the ion to electron temperature ratio (T_i/T_e) is roughly conserved by the entry, energization, heating, and transport processes. This intriguing and seemingly "conserved" property deserves close and careful examinations. Unlike entropy, there has not been a physical argument for the conservation of T_i/T_e ratio. It is not clear what causes the T_i/T_e ratio conservation, if it is conserved, and if T_i/T_e ratio can really serve as a constraint on the plasma transport across the magnetopause and within the plasma sheet.

Once the solar wind plasma enters the magnetotail, it will be distributed throughout the plasma sheet by the transport processes within the magnetotail or plasma sheet. The plasma can get heated and energized during these processes. Some of the transport processes such as curvature and gradient drifts introduce dawn-dusk asymmetries in the particles, especially for the hot component.

During active times, ion outflow rates increase [e.g., *Wilson et al.,* 2001; *Tung et al.,* 2001] and so the plasma sheet heavy ion population can be significant [*Chappell et al.,* 1987; *Schriver and Ashour-Abdalla*, 1990]. *Bouhram et al.* [2005] analyzed Cluster data and found that O^+ density is significantly higher on the duskside than the dawnside of the magnetosphere near the magnetopause. **Lund** [PET, 2009] discussed parameterization of ion outflows using a kinetic model for wave particle interactions. **Peterson** [*Peterson*, 2009; PET, 2009] discussed the importance of in-transit populations for ionospheric outflow. A substorm epoch study of plasma sheet populations also revealed an increase in cold ion densities following about 30 minutes after substorm onset [*Wing and Johnson*, 2009], and this population likely is of ionospheric origin.

Ion outflows or more precisely the presence of the heavy ions may affect the transport processes within the plasma sheet such as magnetotail convection and reconnection [e.g., **Winglee et al.,** 2002].

Heavy ions can affect reconnection at the magnetopause by reducing the Alfvén velocity leading to a slower reconnection rate [*Shay and Swisdak*, 2004]. The study of *Karimabadi et al.* [2011] suggests that heavy ions only affect the reconnection rate when they are the primary current carrier, but that in the nonlinear stage a proton-dominated current sheet can be replaced by heavy ions in the surrounding plasma leading to reduced reconnection efficiency, reduction in the production of secondary islands, and broadening of the reconnection structures.

Kelvin-Helmholtz instability is also significantly affected by the presence of heavy ions. When heavy ions are present at the magnetopause, the plasma density can be increased leading to a reduction of Alfvén velocity and reducing the stabilizing force of the magnetic tension. However, MHD simulations suggest that oxygen stabilizes KH simulations on the flanks—possibly by thickening the boundary layer [**Merkin**, PET, 2010]. The effect of heavy ions on K-H stability in MHD simulations remains a topic of interest. On the other hand, hybrid simula-

tions [**Delamere**, 2010; PET, 2010] suggest that the inertia of heavy ions causes the heavy particles to decouple from field lines so that they decouple from the vortex motion leading causing stabilization and mixing.

Kinetic Alfvén waves are also affected by heavy ions. The ion polarization velocity is larger for heavy ions, leading to larger density perturbations, which require larger parallel electric fields to maintain quasineutrality. This effect leads to larger transport coefficients for all species. However, heavy ions have a lower thermal velocity than light ions (assuming a similar temperature), so a much smaller fraction of heavy particles would be resonant with the kinetic Alfvén wave leading to a barrier to transport of heavy ions across the magnetopause [**Johnson**, PET, 2010].

In the following sections, we will discuss and review (a) plasma sheet filling rate; (b) dawn-dusk asymmetry; (c) entropy; and (d) T_i/T_e ratio and how they can discriminate the three entry mechanisms. Then, we will discuss the transport within the plasma sheet. We will end with a summary and conclusion.

2. Plasma transport across the magnetopause (solar wind entry)

2a. Plasma sheet filling rate

In the discussion of which entry mechanism(s) are significant in filling of the plasma sheet with solar wind plasma, it is useful to establish first whether each entry mechanism is able to explain the observed plasma sheet filling rate. In other words, how much of the observed filling rate can be attributed to each entry mechanism. In an attempt to do this, **Wing et al.** [2006; PET, 2007] selected an event in which IMF is northward for almost 24 h, providing a rare opportunity to monitor the filling of the plasma sheet with cold dense ions. They found that all three mechanisms are capable of filling the plasma sheet with the observed filling rate. However, there is a difference in the dependence of the entry rate on the magnetosheath density (nsh). As shown in eqs. (1) and (2), the double cusp reconnection entry rate is ~ $n_{sh}^{0.5}$ whereas the diffusive entry rate (either KHI or KAW) is ~ n_{sh}. This dependency has not yet been observationally verified.

The results in *Wing et al.* [2006] are consistent with double cusp reconnection studies [e.g., *Øieroset et al.,* 2005] and KHI studies [e.g., *Nykyri and Otto*, 2004; *Nykyri et al.,* 2006], which showed that double cusp reconnection or KHI is sufficient to fill the plasma sheet with cold dense ions, respectively. **Lemon** [PET, 2009] modeled the filling of the plasma sheet during northward IMF using a Lorentz particle tracking code. In their model, plasma sheet temperatures decrease with time and achieve steady state in 3 hours.

2b. Dawn-dusk asymmetries

Global asymmetries in plasma sheet profiles can provide a significant constraint on plasma entry. *Fujimoto et al.* [1998] showed that in Geotail observations, during northward IMF, ions frequently have two components (a hot and a cold component) on the dusk flanks, but only one component with a broad peak on the dawn flank, as shown in Figure 5. Moreover, *Hasegawa et al.* [2003] reported that Geotail observations show that the ion hot component is frequently nearly isotropic on both the dusk and dawn flanks. However, the cold component, which is similar to the magnetosheath ion population, is heated in the direction perpendicular to the magnetic field on the dawnside while it remains isotropic on the duskside, as shown in Figures 6a and 6b [*Hasegawa et al.,* 2003]. In their followed up study, *Hasegawa et al.* [2004a] performed a statistical study on the ion properties on both flanks. The results are shown in Figure 7 (from *Hasegawa et al.* [2004a]). When the ions have clear two components, one component with $T_h > 3$ keV and $T_c < 3$ keV, they are plotted as red and green dots respectively. However, when the ions have just one peak, then they are plotted as black dots. Figure 7 shows statistically that

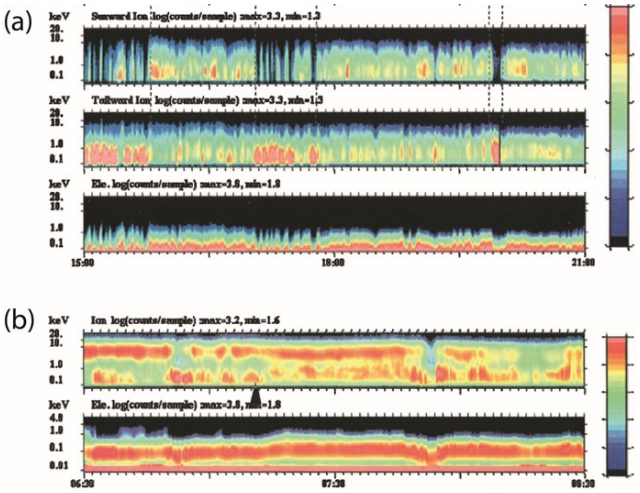

Figure 5. (from *Fujimoto et al.,* 1998])

ions frequently have two components on the duskside, but only one component on the dawnside. The cold component of the electron (temperature less than a few hundred eVs) has been heated in the direction parallel to the magnetic field line [*Hasegawa et al.,* 2003; *Fujimoto et al.,* 1998].

Wing et al. [2005] used DMSP satellites to infer plasma sheet temperatures and densities during periods of northward IMF. They fitted the ion spectra to one-component Maxwellian, two-component Maxwellian, and Kappa distributions and selected the best fits. Their cold component density and temperature profiles are displayed in Figures 6c and 6d, respectively. The cold component density profile has peaks at dawn and dusk flanks, as shown in Figure 6c. This suggests that the source of the cold component is magnetosheath or LLBL. In contrast, the hot component ion density profile does not have peaks at the flanks (see Figure 8 in *Wing et al.* [2005]), which would be expected if the source of the hot component is not the solar wind. Interestingly, the density of the cold component is higher on the dawnside than that on the duskside, suggesting perhaps there are more solar wind ion entry on the dawnside than on the duskside of the magne-

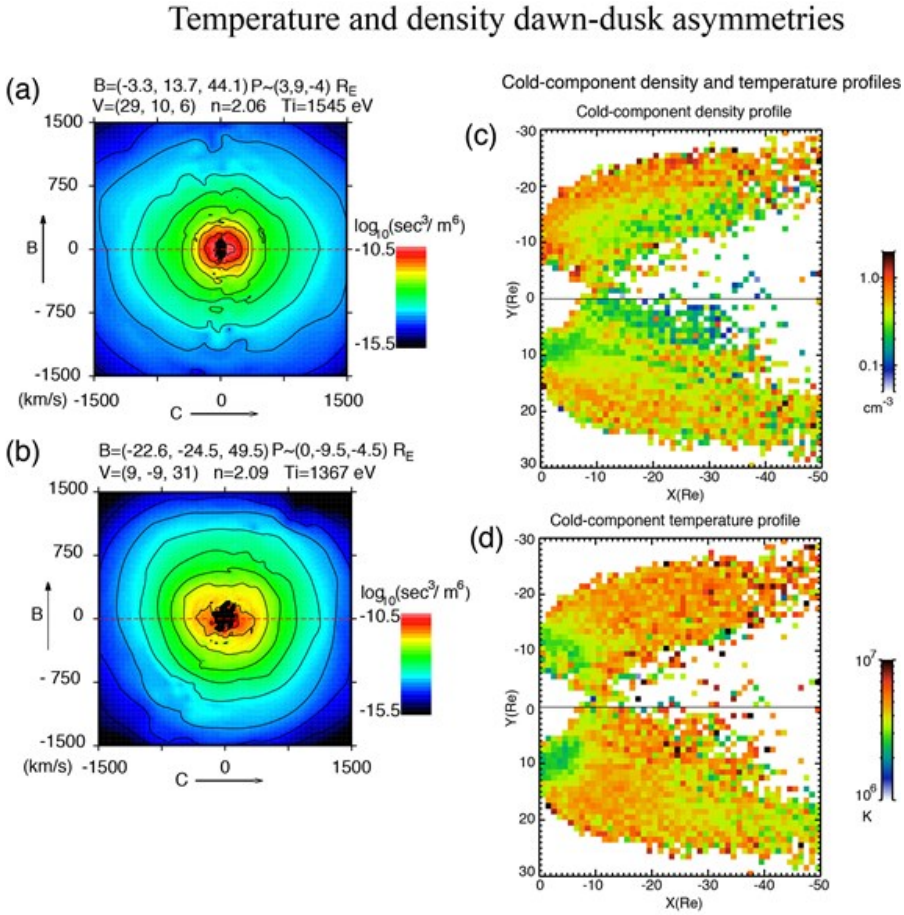

Figure 6. (a) and (b) (from *Hasegawa et al.* [2003]) and (c) and (d) (from *Wing et al.* [2005]).

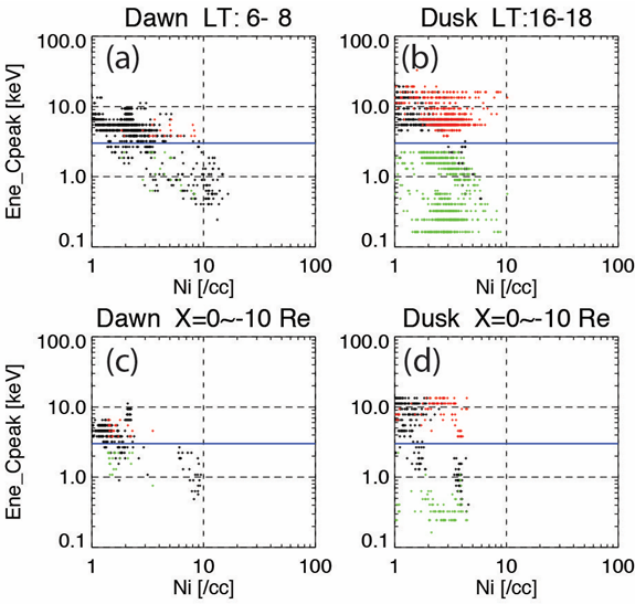

Figure 7. (from *Hasegawa et al.* [2004a]).

topause (see also *Guild et al.* [2008] and **Nagata et al.** [2007; PET, 2007]). Figure 6d shows that the cold component temperatures are higher on the dawnside than the duskside, consistent with *Hasegawa et al.* [2003]. This observation suggests that the magnetosheath ions have been heated in the entry process on the dawnside.

It is not clear what causes the temperature asymmetry in the cold ion profile. For the solar wind Parker spiral, which is the dominant solar wind orientation, the magnetosheath magnetic field has been shown to be more turbulent or have more fluctuations or down stream of the quasi-parallel shock (the dawnside magnetosheath) than down stream of the quasi-perpendicular shock (the duskside magnetosheath) [**Petrinec**, 2013; GEM, 2009]. The fluctuations in the magnetic field could indicate the presence of the compressional waves. KAW can be generated when the compressional waves interact with the magnetospheric boundary, which can lead to diffusive transport of the solar wind/magnetosheath ions across the magnetopause boundary [*Johnson and Cheng*, 1997]. The waves have a parallel electric field, which can heat electrons in the direction of the magnetic field [*Hasegawa and Chen*, 1975; *Hasegawa and Mima*, 1978]. When the waves have large amplitudes, they can also heat ions in the direction perpendicular to the magnetic field [*Johnson and Cheng*, 2001]. Because the source of compressions could be compressional instabilities generated in the magnetosheath or compressions driven directly by the solar wind, in a statistical sense, there can be a dawn-dusk asymmetry in the KAWs and ion heating during entry. A recent survey of wave power in the sheath and magnetopause suggests that the wave power associated with tranvsverse KAWs is enhanced along the dawn flank [*Yao et al.,* 2011], which would provide enhanced transport. The study of *Chaston et al.,* [2008] also provides observational evidence of stochastic heating of ions by KAWs as predicted by *Johnson et al.* [2001].

It is not clear what causes the dawn-dusk asymmetry in the cold ion density profile either. The dawn-dusk density asymmetry can be caused by the dawn-dusk asymmetry in the source, i.e., magnetosheath population itself, or by a dawn-dusk asymmetry in the entry rate. Several magnetosheath studies showed that that the magnetosheath n is higher on the dawnside than the duskside [e.g., **Petrinec**, GEM, 2009; *Paularena et al.,* 2001, *Nemecek et al.,* 2002]. More interestingly, *Walsh et al.* [2012] found that in THEMIS observations, near noon, the magnetosheath density is essentially dawn-dusk symmetrical, n_{dawn}/n_{dusk} ~ 1, but n_{dawn}/n_{dusk} ratio grows larger away from noon, reaching ~1.2 at 5 h away from noon. They also found similar patterns in BATS-R-US MHD, except that the asymmetry is even more pronounced, ~ n_{dawn}/n_{dusk} ~ 1.5, near dawn and dusk flanks. This new result may put an additional constraint on the entry location of the magnetosheath ions. That is, if the source of the magnetospheric cold ion dawn-dusk density asymmetry is magnetosheath, then the magnetosheath source would have to be located several hours away from noon rather than close to noon.

The dawn-dusk asymmetry in the cold ion density may be attributed to the dawn-dusk asymmetry in the entry rate or entry

process, i.e., the entry rate at the dawn flank magnetopause is higher than that at the dusk flank. *Hasegawa et al.* [2006] examined the occurrence rate of the KHI on the dawn and dusk flanks and found that the occurrence rate is roughly equal. However, **Wang et al.** [2007; PET, 2007] reported that the magnetosheath ion entry from the dawn flank is more efficient with decreasing V_{sw}, but no significant V_{sw} effect is seen on the dusk flank. This may suggest that another entry mechanism besides KHI can play a significant role on the dawnside magnetopause. The asymmetric heating of the cold component/magnetosheath ions may suggest an asymmetry in the KAW led entry, i.e., more KAW led entry on the dawnside than the duskside magnetopause.

Asymmetry may also result in K-H waves because of differences in the diamagnetic drift on the two flanks [*Wilber and Winglee*, 1995], through effects of heavy ions [**Johnson**, PET, 2009], or by differences in field-line draping at the flanks.

Olson and Pfitzer [1985] proposed that gradient drift entry (GDE) would allow magnetosheath ions to enter along the dawn flank and the electrons along the dusk flank. They argued that this entry mechanism can lead to the observed FAC polarity and the dawn-dusk current in the magnetotail, at least qualitatively. However, it is not clear if GDE alone can account for the observed filling rate or the cold dense state of the plasma sheet. *Treumann and Baumjohann* [1988] calculated that only 5% of the magnetosheath particles that come in contact with the magnetopause can be trapped in the magnetosphere in their model. The difficulty here is that the number of particles that come in contact with the magnetopause is unknown in any realistic magnetopause model. Hence, the efficiency of GDE is unknown. *Richard et al.* [1994] traced thousands of ions in a fixed MHD electric and magnetic fields and found that most solar wind ions enter the magnetosphere through double cusp type reconnection [*Song and Russell*, 1992] and only a small fraction enters with GDE mechanism. More recently, *Zhou et al.* [2007] used a simple model to calculate GDE efficiency and found that only electrons and ions having energies larger than several keV can gradient drift into the magnetosphere during southward IMF. However, during northward IMF, lower energy particles can enter, but their efficiency was not calculated. In any case, GDE cannot explain the ion and electron heating in the entry process. Although GDE itself has not been attributed to heat particles, the mechanism can be effective at moving hot particles. For example, *Øieroset et al.* [2008] observed hot and cold components on the same field line in the dayside magnetosphere. They attributed the cold component to magnetosheath ions from either poleward of the cusp double reconnection or poleward of the cusp in one hemisphere and equatorward of the cusp in the other hemisphere. However, they attributed the hot component to magnetospheric ions that have curvature and gradient drifted into the newly closed field lines.

The dawn-dusk asymmetry in the solar wind entry rate may also be attributed to the asymmetry in the magnetotail flank reconnection. **Peroomian and El-Alaoui** [2008; PET, 2007] performed large-scale kinetic (LSK) simulations that show that most solar wind ions enter along the dawn flank primarily through reconnection. They also found that the entry locations can be modulated by IMF *By* [**Peroomian**, PET, 2007]. When IMF *By* is positive, the solar wind ion entrees along the dusk flank can increase. Similarly, using the same technique, *Peroomian et al.* [2011] showed that a large number of solar wind ions enter along the dawn flank through reconnection and get energized nonadiabatically before reaching the dawnside ring current. LSK shows the the magnetic field line configuration can be very complex and entertwined [**Peroomian**, PET, 2010].

Li et al. [2008; PET, 2008] studied the double cusp reconnection entry mechanism with MHD and found that ionospheric conductance affects the convection of the

newly closed field lines and can change the solar wind entry rate and introduce asymmetry in the entry rate. However, this mechanism may not introduce dawn-dusk asymmetry in the cold component temperature, although asymmetries in MHD simulations may also result from local time differences in ionospheric conductances [*Zhang et al.,* 2012] During southward IMF, there is evidence that solar wind particles can still enter from the flank magnetopause albeit at smaller quantities. Figure 8 panels a–d show plasma sheet ion n and T profiles for northward and southward IMF obtained from DMSP observations (note here the hot and cold components are combined) [*Wing and Newell*, 2002]. Panels a and b show that during northward IMF, there are density maxima and temperature minima along both flanks, which can be taken as a signature for solar wind ion entrees, as discussed above. Interestingly, during southward IMF, there is also evidence for solar wind ion entry along the flank, as suggested by the density maxima and temperature minima along both flanks in panels c and d, albeit the density maxima and the temperature minima are smaller compared to those for northward IMF. These DMSP observations are corroborated in Geotail observations in panels e – h, which show that during southward IMF, there are density peaks and temperature minima on both flanks, but the flank source is weaker [**Wang et al.**, 2006; PET, 2007]. Presently, it is not firmly established what is/are the entry mechanism(s) for solar wind ions to enter along the flanks during southward IMF, but KHI and KWA, in principle, can still operate under southward IMF, although KHI may be less favorable for southward IMF [*Miura*, 1995]. **Lyon** [PET, 2008; 2009; 2010] showed that in LFM simulations, KH waves are present in the flanks for both northward and southward IMF. The cold ions are transported toward the midnight meridian through interchange instability, which appears as "fingers" in LFM density profiles. Recently, **Hwang et al.** [2011; PET, 2009] observed KH waves under southward IMF on the dawnside, but the KH vortices can be irregular and intermittent.

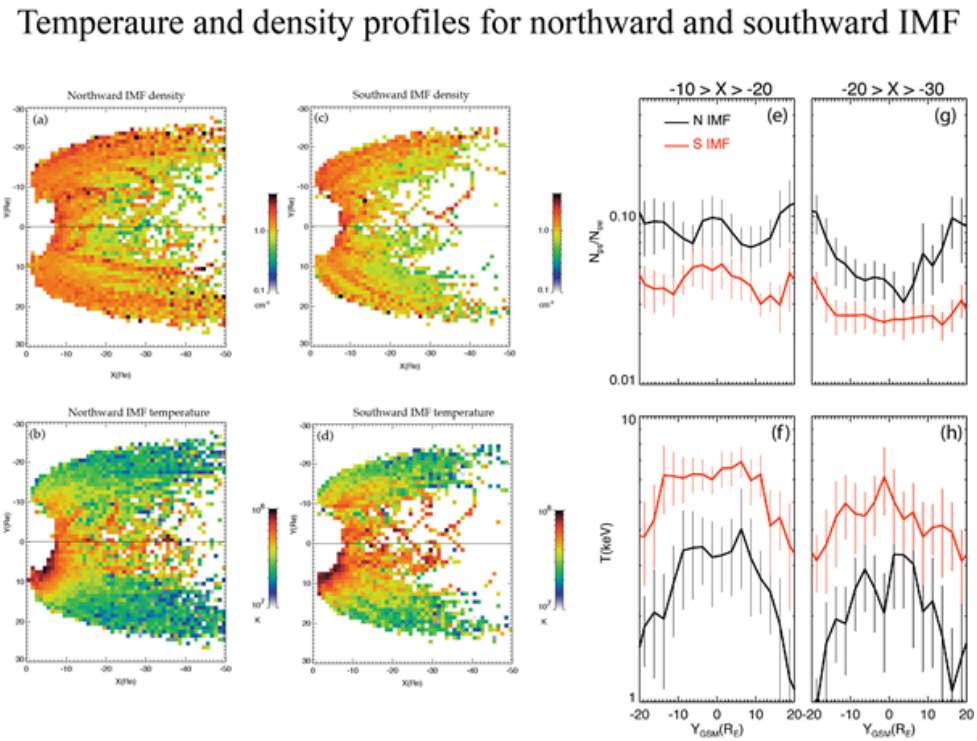

Figure 8. (a) – (d) (from *Wing and Newell* [2002]) and (e) and (f) (from *Wang et al.*, PET09 Workshop, Fairbanks, Alaska, March 2009; the method is described in *Wang et al.* [2010]).

2c. Entropy

For studies of transport of plasma into and within the plasma sheet, it is often useful to consider what parameters are conserved and under what conditions. One fundamental conserved quantity is the entropy, which is conserved both locally and globally when the plasma response is adiabatic [*Birn et al.,* 2006b].

More detailed discussion and application of entropy can be found in the 2009 JGR special section on *"Entropy Properties and Constraints Related to Space Plasma Transport"* guest edited by the authors (see *Wing and Johnson* [2010] and references therein).

Specific entropy, $s=p/\rho^{\gamma}$, places significant constraints on plasma entry mechanisms. Figure 9a shows that statistically the magnetosheath ion s is 2 – 3 orders of magnitude lower than plasma sheet ion s. Hence, it would be expected that a signature of the solar wind entry is to lower s in the plasma sheet. This is indeed observed, as shown in Figure 9b, which shows that s is lower in both flanks, where there is a higher concentration of cold (solar wind) ions [*Wing et al.*, 2005], than that near midnight meridian. Figure 9c suggests that there is a duskward heat flux in the hot ions entropy profile, as would be expected from the curvature and gradient drifts. Figure 9 illustrates two interesting and relevant points: (1) during entry, solar wind ion specific entropy increases by 2 – 3 orders of magnitude (Figure 9a); and (2) upon entry, the transport process that moves cold ions from the flanks to near midnight increases the specific entropy further by a factor of ~5 (Figure 9d). Point (2) can be crucial in resolving another key issue: what process transports cold plasma from the flanks to the midnight meridian. Figure 9d suggests that whatever the process may be it would need to increase the specific entropy by a factor of ~5.

The total flux-tube entropy, $S=p^{1/\gamma}V$, where V is the flux tube volume (or the more general intergral form) provides an important constraint on the source of plasma

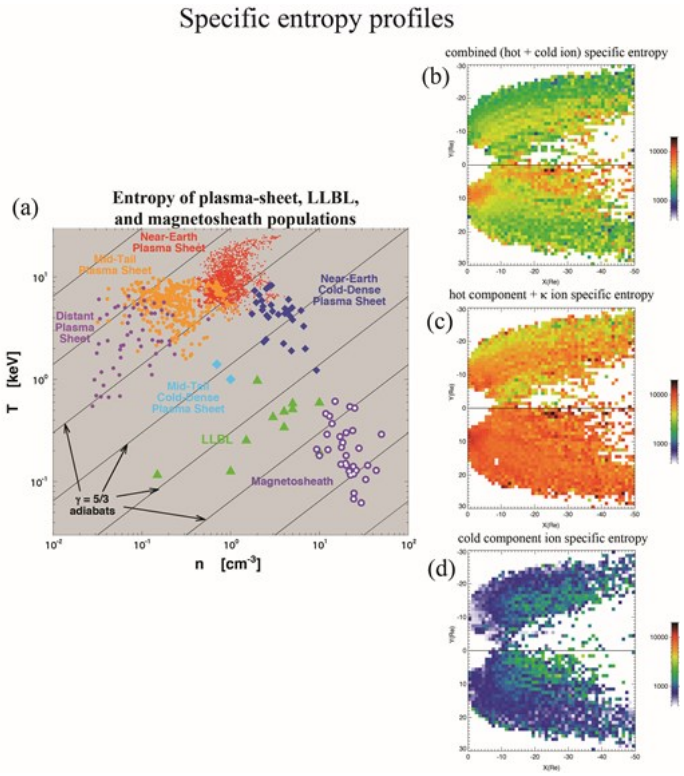

Figure 9. (from *Johnson and Wing*, [2009]). (a) (courtesy of Joe Borovsky).

sheet material, because once material is captured on closed flux tubes it should satisfy the entropy constraint if it is convected adiabatically into the plasma sheet. This value of this constraint, S, can be estimated from solar wind conditions and assumptions about the plasma capture process and compared with typical values in the plasma sheet. Total entropy does not increase significantly for double cusp reconnection [*Johnson and Wing*, 2009; **Adamson**, PET, 2009], but it may increase significantly for reconnection in Kelvin-Helmholtz vortices. Moreover, the observed increase of plasma temperature tailward along the flanks is also inconsistent with entropy conservation of plasma captured by double-cusp reconnection, which implies that nonadiabatic processes leading to plasma loss and/or heating are required in order for plasma captured by double cusp reconnection to reach the plasma sheet [*Johnson and Wing*, 2009].

Local changes in entropy may be associated with wave-particle interactions, heat fluxes of captured populations, and other dis-

sipative mechanisms. Possibly several mechanisms are responsible for the change in entropy. Three-dimensional simulations of shear flow instabilities show that magnetic reconnection can mix magnetosheath and magnetosphere population leading to reduced entropy on closed field line region. Eddy diffusion and kinetic drifts can also affect the entropy profiles in the plasma sheet.

2d. Ion to Electron Temperature Ratio (T_i/T_e)

Another important observational "constraint" on solar wind entry and plasma transport processes in the plasma sheet is the rough, not exact, preservation of the temperature ratio of ions and electrons, T_i/T_e. For example, *Baumjohann et al.* [1989] reported that $5.5 < T_i/T_e < 11$ in the plasma sheet. T_i/T_e has been shown to have a dependence on solar wind Alfvén Mach number (M_A). For example, **Lavraud et al.** [2009; PET, 2009] examined an event in which M_A is low, ~ 8, and found that Ti/Te is also unusually low ~ 3. *Wang et al.* [2012] found a similar dependence on solar wind velocity.

The ratio of T_i/T_e changes significantly at the bow shock and is determined by solar wind parameters. However, it is particularly interesting that the solar wind entry process appears to roughly conserve the T_i/T_e of the magnetosheath particles during the transport across the magnetopause [**Borovsky**, PET, 2010]. This property can be seen in Figure 10a, which shows that $5 < T_i/T_e < 10$ in the magnetosheath and plasma sheet. Within the magnetosheath, T_i/T_e remains the same as the particles flow downstream and cool adiabatically, as would be expected. Figures 10b and 10c show two events in which THEMIS crossed from the magnetosheath to the plasma sheet. Both figures show that T_i/T_e of the magnetosheath (green line in the third panel from the top) appears to be similar to the T_i/T_e of the cool plasma (blue line in the third panel from the

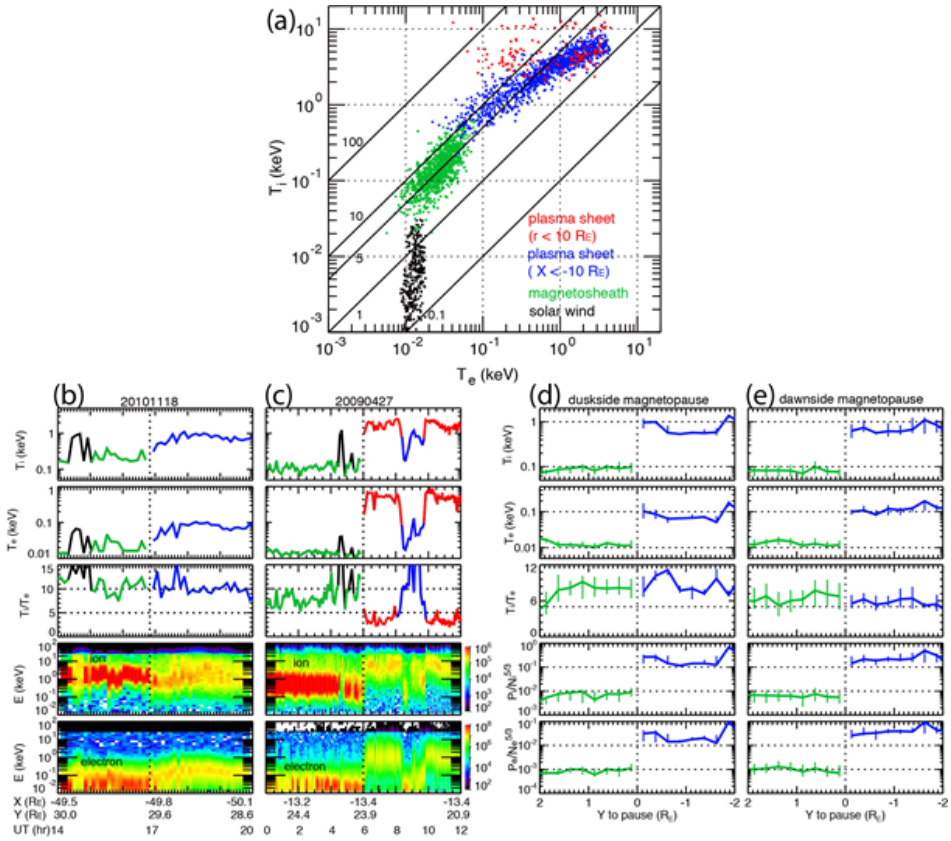

Figure 10. (a) (from Figure 1 in *Wang et al.* [2012]) and (b) – (e) (from Figure 8 in *Wang et al.* [2012]).

top). Figures 10d and 10e show statistically T_i/T_e of the magnetosheath and the cool plasma (not necessarily cold component, although it should be dominated by cold component) on both sides of the dusk and dawn magnetopause, respectively, at $X < -40$ R_E. Figures 10d and 10e suggest that when ions and electrons cross the magnetopause boundary from the magnetosheath to the magnetosphere, T_i and T_e increase by a factor of ~ 6 to 10 and specific entropies, si and se increase by a factor of ~20. *Wang et al.* [2012] interpreted these changes as the signature of a non-adiabatic heating process at the boundary that heats the ions and electrons by the same proportion.

Within the plasma sheet, there is a strong dawn-dusk asymmetries in T_i/T_e which can be attributed to the curvature and gradient drift such that T_i (T_e) is higher at the dusk (dawn) [e.g., *Wang et al.,* 2012]. Hence, T_i/T_e would have dependence on the locations. *Kaufmann et al.* [2005] found that T_i/T_e increase earthward near midnight meridian. They offered several possible explanations: (1) electrons proportionally gain more energy than ions; (2) the ions lose energy through parallel heat flux to the ionosphere by radiating Alfven waves; (3) magnetic reconnection can heat ions and electrons differently. Fast flows can reduce ion density, but increase ion temperature. Because of these, *Kaufmann et al.* [2005] suggested that the factors influencing T_i/T_e variability can be more complicated than just curvature and gradient drifts. The nearly constant T_i/T_e suggests that ions absorb 5 – 10 times as much heat as the electrons in the plasma sheet [e.g., *Kaufmann and Paterson*, 2009].

In one of a few theoretical and modeling studies that try to explain T_i/T_e, *Schriver et al.* [1998] modeled ion and electron acceleration in the magnetotail by following trajectories of thousands of particles in T89 magnetic field model [*Tsyganenko*, 1989] and a constant dawn-dusk electric field of 0.25 mV/m in the magnetotail. They obtained $T_i/T_e = 4 - 6$. To explain this ratio, they derived an expression of $T_i/T_e = (m_i/m_e)^{1/3} (B'_e/B'_i)^{2/3}$ where B' = the magnetic field gradient where the electron or ion first crosses the neutral sheet. Hence, to obtain the observed T_i/T_e, they would require ions to cross the neutral sheet closer to Earth than electrons.

3. Plasma transport within the plasma sheet

3a. ExB, curvature and gradient drifts

Two transport mechanisms that have been shown to play significant roles in the plasma sheet and that have successfully explained large scale features in the plasma sheet are (1) ExB and (2) curvature and gradient drifts. For example, Figure 8 panels a – d show that the quiet time or northward IMF ion T and n profiles have the following large scale features: (1) density peaks along both flanks and the inner edge of the plasma sheet: (2) temperature peak at the dusk-midnight sectors at the inner edge of the plasma sheet ($r = 8 - 10$ R_E); and (3) temperature minima along both flanks [*Wing and Newell*, 1998; 2002; *Wing et al.,* 2005; *Johnson and Wing,* 2009]. These large scale features have also been observed with in situ observations [*Wang et al.,* 2001; 2006]. These features can be attributed to two plasma sources: (1) cold ions from the LLBL, and (2) hot ions from deep tail; and two transport mechanisms: (1) ExB and (2) curvature and gradient drifts [e.g., *Spence and Kivelson*, 1993; *Wang et al.,* 2001; 2006; *Wing and Newell,* 1998; 2002; *Wing et al.,* 2005]. Cold ions that enter the plasma sheet from the flanks mostly ExB drift sunward, resulting in temperature minima and density maxima along both flanks. The hot ions ExB sunward while curvature and gradient drifting westward, especially in the near-Earth region where the magnetic field is stronger ($r < 10$ R_E), leading to the temperature peak at the dusk-midnight sector at the inner edge of the plasma sheet. The importance of the magnetic drift increases whereas the importance of ExB drift decreases with decreasing dis-

tance from Earth. By the time the particles reach the inner magnetosphere, ExB drift is negligible as curvature and gradient drifts dominate [*Wang et al.,* 2004]. As a result, the ions and electrons mainly move azimuthally, with the ions moving westward while the electrons eastward. As they circle around the Earth, some of the ions and electrons precipitate into the ionosphere [*Wing et al.,* 2013]. **Lyons** [PET, 2009] showed examples of strong convection for northward IMF associated with fluctuating IMF conditions that are mostly associated solar wind high speed streams.

As shown in Figure 8, relative to northward IMF, during southward IMF: (1) fewer solar wind ions enter along the flanks and (2) the stronger convection and dawn-dusk electric field leads to larger ExB drift. These differences in drifts between northward and southward IMF gives rise to the question what happens when IMF turns southward after a prolonged northward IMF and the plasma sheet has been loaded with cold and dense plasma. *Thomsen et al.* [2003] investigated this phenomenon and found that strong ring current and geomagnetic disturbance can ensue when prolonged northward IMF is followed by strong convection due to southward IMF or a large solar wind dynamic pressure. Basically, when IMF turns southward, the massive preloaded materials in the plasma sheet are delivered to the inner magnetosphere, resulting in strong ring current and large geomagentic disturbance [*Denton et al.,* 2005, *Lavraud et al.,* 2006a]. This is analogous to the calm before storm. **Lavraud et al.** [2006b; PET, 2007] also studied the effect of prolonged northward IMF followed by southward IMF. They found two ion populations at the geosynchronous orbit: (1) midnight and (2) dawnside. The dawnside cold dense ions at the near-Earth plasma sheet during active times or substorm growth phase have been previously observed [*Wing and Johnson*, 2009; *Wing and Newell*, 1998; 2002; *Korth et al.*, 1999; *Denton et al.,* 2005] and modeled [*Wang et al.,* 2004]. It has been attributed to the stagnation point where ExB and corotation is nearly balanced by the curvature and gradient drift [*Friedel et al.,* 2001] and solar wind entry on the dawn flank.

Interestingly, *Ashour-Abdalla et al.* [2010] found that during northward IMF, the plasma sheet can temporarily split into dawn and dusk halves in LSK simulation. They attributed this division to the presence of flux ropes in the center of the tail possibly due to the localized near-Earth reconnection.

Ion outflows during active times can significantly increase plasma sheet O^+ population, which can at times carry much of the energy (e.g. storm-time ring current). Escaping O^+ has higher fluxes in the 00 – 12 MLT (midnight-dawn-noon) sector than 12 -1 24 MLT (noon-dusk-midnight) sector [**Redmon et al.**, 2012; PET, 2009; *Collin et al.,* 1988]. This may be related to the observations of cold dense ions in the plasma sheet post-midnight sector after substorm onset [*Wing et al.*, 2007; *Wing and Johnson*, 2009]. Observations of O^+ outflow during storm and substorm in the magnetotail suggest that cusp was the source and that the southern hemisphere has higher frequency of O^+ outflows than northern hemisphere [**Kistler**, PET, 2010]. There was evidence of O^+ heating [**Zhang**, PET, 2010] and the solar EUV controls H^+ and O^+ outflow densities [**Moukis**, PET, 2010]. These outflows (combined with associated energization processes) could significantly modify the background plasma and magnetospheric ExB convection [e.g., *Winglee et al.,* 2002]. Several important physical effects might be expected. MHD simulations show that dayside O^+ outflows may move the X-line closer to Earth in order to maintain the same reconnection rate on the dayside [e.g., *Brambles, et al.,* 2010; *Wiltberger et al.,* 2010]. On the other hand, nightside O^+ outflows may have the opposite effect, moving the X-line further from the Earth due to the increased plasma pressure [e.g., *Garcia et al.,* 2010].

3b. Turbulence

Once the solar wind plasma enters the plasma sheet, it can be distributed throughout the plasma sheet. Observations show that the cold dense ions can be found throughout the entire plasma sheet during northward IMF [e.g., *Terasawa et al.,* 1997; *Oieroset et al.,* 2005; *Wing and Newell*, 2002; *Wing et al.,* 2005; *Wing et al.,* 2006; *Johnson and Wing,* 2009]. However, the mechanism for transporting cold dense plasma from the flanks to the midnight meridian (center of the plasma sheet) has not been clearly established or uniformly accepted.

The plasma sheet has been observed to be turbulent, which can play some roles in the plasma transport [*Borovsky et al.,* 1997; *Borovsky and Funsten*, 2003; **Weygand et al.,** 2005; PET, 2009]. One source of the turbulence may be velocity shear instabilities [*Borovsky et al.* 1997]. **Wang et al.** [2010; PET, 2009] performed a simulation that shows that diffusive transport due to turbulence can move cold particles from the flank to the midnight meridian. As such, turbulence is an important process that is intrinsic to the quasi-stable state of the tail and boundary layer [*Antonova*, 2005] as well as its stability [*Stepanova et al.,* 2011].

3c. Entropy

Section 2c. discusses the concept of total entropy, S, and specific entropy, s, and their importance to the solar wind plasma entry problem. It turns out, these two entropy parameters are also relevant for the study of the plasma transport within the plasma sheet. S is an important parameter to identify when the interchange instability is operable. In particular, reductions in S can be significant because they can lead to interchange instability to reach a more stable magnetospheric configuration [*Gold*, 1959; *Sonnerup*, 1963; *Hill*, 1976; *Chen and Wolf*, 1999], which can lead to earthward plasma transport at high speed commonly known as fast flow [e.g., *Pontius and Wolf*, 1990].

Statistical studies have shown fairly definitively that in the magnetotail, S is not conserved — S decreases with decreasing distance from Earth [*Erickson and Wolf*, 1980; *Kaufmann and Paterson*, 2009; *Wing and Johnson*, 2009; **Wang et al.,** 2009; PET, 2010; *Garner et al.,* 2003]. Nonconservation of S can occur in nonadiabatic processes such as wave-particle interactions, heat flux, gradient/curvature drifts [*Tsyganenko*, 1982; *Kivelson and Spence*, 1988; *Wang et al.,* 2001; 2004; *Wolf et al.,* 2009; *Wing and Johnson,* 2009; *Kaufmann and Paterson*, 2008] and non earthward $\mathbf{E} \times \mathbf{B}$ drift [e.g., *Kaufmann et al.,* 2004]. Nonconservation of S can also occur when there is a loss of plasma content in the flux tube [e.g., *Pontius and Wolf*, 1990; *Chen and Wolf*, 1993; *Wing and Johnson*, 2009; *Borovsky et al.,* 1998b]. S and s can also change when plasma is added to the flux tube, e.g., through solar wind plasma entry or ionospheric outflow [e.g., *Johnson and Wing,* 2009]. If the localized process leads to field-line reconfiguration (reconnection), then the change of S is more related to the change of flux tube volume than to changes in s within that volume.

Birn et al. [2006a; 2009; PET, 2009] and *Wing and Johnson* [2009] discussed S changes in flux-tube reconfiguration in magnetic field reconnection process in which the closed field line splits into two parts: (1) a newly closed field line albeit with reduced length and (2) a tailward convecting plasmoid. The newly closed field line has much lower S and V compared to those in the original flux tube, while the remainder resides in the newly formed plasmoid.

An earthward fast flow can attain velocity greater than 400 km/s and has been associated with a bubble, which is a magnetotail flux tube having lower density, pressure, and S than surrounding flux tubes. [e.g., *Sergeev et al.,* 1996; *Nakamura et al.,* 2005; *Angelopoulos et al.,* 1994]. Herein, the term fast flow includes bubble, bursty bulk flow (BBF) and flow burst (shorter duration than BBF). Fast earthward flows can be more frequently observed during magnetically active times and have been associated with substorm onsets and their frequency of

occurrence reaches a peak at the start of the recovery phase [e.g., *Nakamura et al.,* 2002; *Angelopoulos et al.,* 1994; *Baumjohann et al.,* 1990; *McPherron et al.,* 2011; *Sergeev et al.,* 2008; *Slavin et al.,* 2002]. **Erickson** [PET, 2007] showed that *S* has different characteristics for substorms and pseudo breakups. Fast flow observations and simulations often show two parts: (1) the head where B_z is large (the dipolarization front) and (2) the tail. The pressure inside the bubble is smaller than that outside of the bubble. This pressure gradient leads to the field-aligned current with region-1 polarity, whose particle precipitation signature in optical images often appears as an auroral streamer. Thus, many studies pair auroral streamers with fast flows [e.g., *Sergeev et al.,* 2004; *Nakamura et al.,* 2001; *Lyons et al.,* 1999; *Sanchez et al.,* 2012].

Of course, care has to be taken when mapping the observations from the magnetotail to the ionosphere. **Larry Lyons** [PET, 2008] reviewed two main issues in mapping the convection pattern from the magnetosphere to ionosphere: the potential and induced electric fields. The former concerns with the particles crossing the field line whereas the latter concerns with the changing magnetic field. **Baker** [PET, 2008] showed the results of the comparisons of mapping Cluster EDI electric field observations to ionosphere with T96 magnetic field model with SuperDARN convection pattern. He found that 24% of EDI measurements are not accounted by the SuperDARN, but generally there was good agreement.

Ionospheric velocity measurements inferred from Superdarn also suggest that even under steady driven conditions, there are significant ionospheric velocity fluctuations [**Bristow et al.,** 2008; PET, 2009]. They occur for all local times, though are largest in the afternoon sector at auroral latitudes, and the prenoon polar cap. The level of fluctuation seems to be independent of substorm/nonsubstorm conditions. The average time for a significant fluctuation is on the order of ten minutes for all latitudes and local times, and they obey a power law distribution for at least part of its range. The ionospheric fluctuations could be a remote indicator of plasma sheet turbulence, and useful for studies of plasma sheet transport.

There has been no clear picture of the earthward fast flows $r < 10 - 12$ R_E. It appears that many fast flows slow down at $r < 10 - 12$ R_E [e.g., *McPherron et al.,* 2011, *Panov et al.,* 2010a] and many do not reach inner magnetosphere or geosynchronous orbit [e.g., *Ohtani et al.,* 2006]. Observations and theory suggest that in the final stage of the bubble earthward motion, the filamentary bubble executes a damped oscillation about an equilibrium (interchange oscillation) as the bubble slows down and eventually comes to a stop (interchange oscillation) [*Wolf et al.,* 2012; *Panov et al.,* 2010b]. In Rice Convection Model-Equilibrium (RCM-E) simulations, flux tubes do not generally reach in the inner magnetosphere, unless their total entropies (*S*) have been reduced [*Lemon et al.,* 2004; *Zhang et al.,* 2008].

In **Birn et al.** [2009; PET, 2009] simulations, after the reconnection, the newly closed field line, which has smaller entropy and flux tube compared to the surrounding flux tubes, can initiate the unstable growth of ballooning and interchange instability, resulting in the earthward propagation of the flux tube. These bubbles would move earthward until their *S* equals that of their neighbors [*Wolf et al.,* 2009]. The more depleted the flux tube, the closer to Earth it can penetrate. This view has been supported in some recent observational studies [e.g., *Dubyagin et al.,* 2011]. Recently, **Birn et al.** [2011] and [PET, 2010] showed that as bubbles move earthward, vortices of return flow develop and the bubbles also fragment, developing cross-tail structuring in the later stages, as shown in Figure 11. **Birn** [PET, 2009] argued that narrow bubbles also tended to penetrate deeper, although there was an optimum width.

Plasma sheet properties can affect the plasma sheet transport to the inner magnetosphere **Gkioulidou**, [PET, 2007] presented

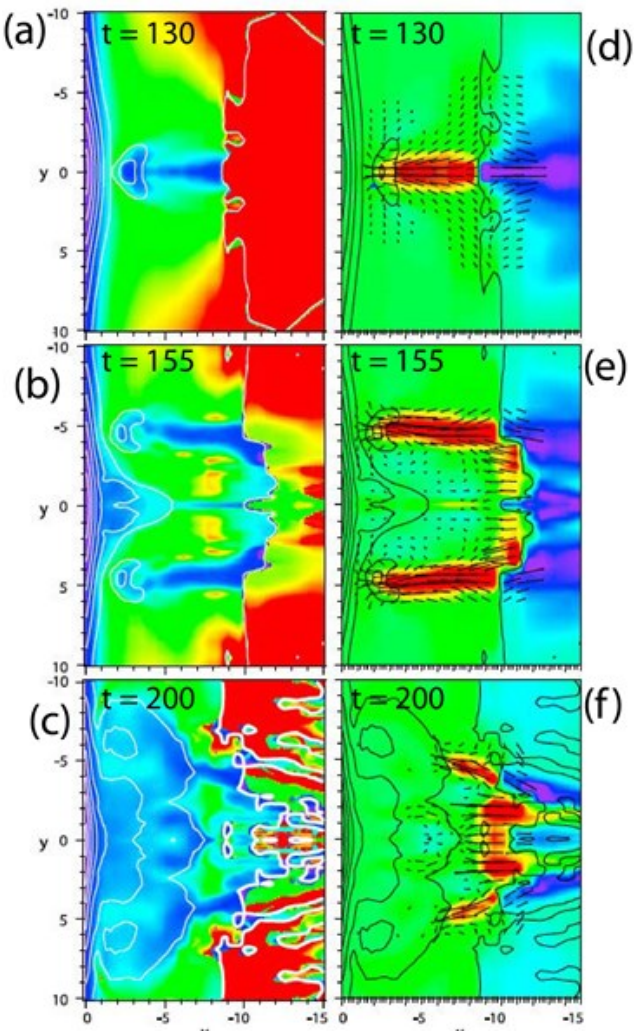

Figure 11. Total entropy, *S*, (a), (b), (c), and flow in the *X-Y* plane (d), (e), and (f) at three different times in *Birn et al.* [2011] MHD simulation.

a simulation that shows that old ions can penetrate into the inner magnetopshere more effectively and enhanced cold ions in the flanks enhances fast flow near midnight. **Nishimura** [PET, 2007] examined a storm event in which the convection is weak in the plasma sheet, but strong in the flanks and inner magnetosphere. **Otto** [PET, 2009] presented an exciting new result showing that convection of flux to the dayside (subject to constraint of entropy conservation) leads to the formation of intense, thin current sheets. **Wilder** [PET, 2009] discussed saturation of the potential across convection cells for northward IMF. The reverse convection potential is smaller in the summer (10 mV/m) than in winter (11.5 mV/m), suggesting that in winter months viscous cells become more important.

Fast flows and *S* may be relevant to plasma transport in other planetary magnetospheres as well. For example, many studies found that the plasma injection at Saturn's magnetopshere is often characterized as having "deep density cavity" where the ions (both protons and water group) and electrons in the injected flux tube have lower densities than those of the surrounding plasma [e.g., *Sittler Jr. et al.,* 2006; *Rymer et al.,* 2009; *Burch et al.,* 2005; *Hill et al.,* 2005; *Sittler Jr et al.,* 2005]. This is exactly what is observed with fast flow and fast flow led plasma injection at Earth's magnetosphere.

At Saturn, distant reconnection, either Vasyliunas or Dungey type reconnection, can lead to the reduction of the flux tube volume and hence *S*. Like at Earth, the entropy depleted flux tube can lead to interchange instability [e.g., *Young et al.,* 2005; *Hill et al.,* 2005] and move inward where the background *S* is lower, but the density can be higher [e.g., *Thomsen et al.,* 2010; *McAndrews et al.,* 2009]. Some Saturn studies have interpreted the density-depleted flux tube as a bubble [e.g., *André et al.,* 2007]. Like at Earth, the bubble would seek a path to the region where the background *S* is lower, which means that it would move inward. An interesting variation of the process for Saturn may be that as a bubble moves inward in the inner magnetosphere it encounters colder neutrals and ions may undergo charge exchange. This may reduce the entropy of the bubble even more and perhaps allow it to penetrate deeper into Saturn's inner magnetosphere.

4. Summary and Conclusion

This paper reviews our current understanding of the plasma transport from the solar wind to the magnetotail and plasma transport within the magnetotail. Three solar entry mechanisms are examined for

northward IMF solar wind entrees: (1) double cusp reconnection [*Song and Russell*, 1992], (2) KHI [e.g., *Otto and Fairfield*, 200], and (3) KAW [*Johnson and Cheng*, 1997]. In order to determine, which of these three mechanisms can play the most significant roles and under what conditions, we examined four observational constraints: (1) plasma sheet filling rate; (2) dawn-dusk asymmetries; (3) specific and total entropies; and (4) T_i/T_e.

It turns out that all three mechanisms are capable of filling the plasma sheet with cold dense plasma. The entry rate from each mechanism is quite similar and consistent with the observed filling rate in an event that *Wing et al.* [2006] examined. However, the dependence of the filling rate on solar wind density can potentially be used to discriminate double cusp reconnection vs. KHI or KAW. Double cusp reconnection entry rate is proportional to ~nsh05 whereas KHI or KAW entry rate is proportional to ~n_{sh}.

In situ and remote observations of the cold component (magnetosheath/solar wind origin) ions at the plasma sheet flanks near the magnetopause reveal that the cold component density and temperature are higher on dawn flank than those on the dusk flank. In situ observations show that while on the duskside, the ion hot (magnetospheric origin) and cold component temperatures are isotropic, on the dawnside, the ion cold component appears to have been heated in the direction perpendicular to the magnetic field and the electrons have been heated in the direction parallel to the magnetic field. These are consistent with the expected signature of the KAW interaction with particles. On the duskside, the ions are frequently observed to have two components whereas on the duskside, the ions are frequently observed to have one component. The hot component has higher temperature on the duskside than the dawnside because of the curvature and gradient drifts. In contrast, the cold component has higher temperature on the dawnside than the duskside. As a result, on the duskside, the hot and cold components are often easily identified whereas on the dawnside, the hot and cold component temperatures are often close to each other and the ions are often seen as having one component with a broad peak.

The higher density of the cold component on the dawnside magnetotail may result from the dawn-dusk asymmetry of the magnetosheath ion density (magnetosheath ion density is higher on the dawnside than the duskside). The higher density of the cold component of the dawnside magnetotail may also result from a dawn-dusk asymmetry of the entry rate.

The solar wind/magnetosheath entrees reduce the specific entropy (s) of the plasma sheet ions. The cold component s increases by a factor of 5 from the flanks to the midnight meridian. So, whatever mechanism that transport the cold ions from the flanks to the midnight meridian has to explain this increase in *s*.

T_i/T_e appears to be roughly conserved when the magnetosheath particles are transported across the magnetopause boundary to plasma sheet even though both T_i, T_e, s_i and s_e increase significantly. This suggests non-adiabatic heating during entry.

Within the magnetotail, ExB and curvature and gradient drifts play important roles in the plasma transport and can explain the large observed features of the *n, T, p* profiles. Turbulence can also play a significant role, particularly in transporting cold plasma from the flanks to the midnight meridian. Ion outflows can change the magnetotail convection and reconnection location. Total entropy, *S*, and fast flows can play significant roles in the sunward transport. Many fast flows do not reach the inner magnetosphere, but simulations show that fast flows would only travel inward until its *S* matches the background *S*. Total entropy, *S*, can also play a significant role in other planetary magnetospheres.

Acknowledgments. We thank GEM committee for supporting the PET Focus Group (FG). We also thank all the participants of

the PET FG for their invaluable contributions. We also thank NSF for supporting our PET 09 Conference in Fairbanks, Alaska. Simon Wing gratefully acknowledges support from NSF Grants ATM-0802715, and AGS-1058456 and NASA Grant NNX13AE12G. Jay Johnson was funded by NASA grants (NNH09AM53I, NNH09AK63I, and NNH11AR07I), NSF Grants ATM0902730 and AGS-1203299, and DOE contract DE-AC02-09CH11466. We also acknowledge the support of the International Space Science Institute (ISSI) International Teams Program, which made it possible for a small team of scientists to convene and have in-depth and informal discussions on topics relevant to PET FG.

References

Anderson, B. J., and S. A. Fuselier (1994), Response of thermal ions to electromagnetic ion cyclotron waves, *J. Geophys. Res., 99*, 19413-19425.

André, N., et al. (2007), Magnetic signatures of plasma-depleted flux tubes in the Saturnian inner magnetosphere, *Geophys. Res. Lett., 34*, L14108, doi:10.1029/2007GL030374.

Angelopoulos, V., C. F. Kennel, F. V. Coroniti, R. Pellat, H. E. Spence, M. G. Kivelson, R. J. Walker, W. Baumjohann, W. C. Feldman, J. T. Gosling, and C. T. Russell (1993), Characteristics of ion flow in the quiet state of the inner plasma sheet, *Geophys. Res. Lett., 20,* 1711-1714.

Angelopoulos,V., et al. (1994), Statistical characteristics of bursty bulk flow events, *J. Gelphys. Res., 99*, 21,257 – 21,280.

Angelopoulos, V. (1996), The role of impulsive particle acceleration in magnetotail circulation, *Proc. Third International Conf. on Substorms (ICS-3)*, Versailles, France, 12-17 May 1996, ESA SP-389.

Antonova, E. E. (2005), The structure of the magnetospheric boundary layers and the magnetospheric turbulence, *Planet. Spa. Sci., 53,* 161-168, doi:10.1016/j.pss.2004.09.041.

Ashour-Abdalla, M., J. M. Bosqued, M. El-Alaoui, V. Peroomian, and R. Walker (2010), Observations and simulations of a highly structured plasma sheet during northward IMF, *J. Geophys. Res., 115*, A10227, doi:10.1029/2009JA015135.

Baumjohann, W., G. Paschmann, and C. A. Cattell (1989), Average plasma propertis in the central plasma sheet, *J. Geophys. Res., 94*, 6597.

Baumjohann, W., G. Paschmann, and H. Luhr (1990), Pressure balance between lobe and plasma sheet, *Geophys. Res. Lett., 17,* 45-48.

Baumjohann, W. (1993), The near-Earth plasma sheet: An AMPTE/IRM perspective, *Spa. Sci. Rev., 64*, 141–163.

Baumjohann, W., and R. A. Treumann (1997), *Basic Space Plasma Physics*, p. 120, Imperial College Press, London, U. K..

Baker, D. N., E. W. Hones, Jr., P. R. Higbie, and R. D. Belian (1981), Global properties of the magnetosphere during a substorm growth phase: A case study, *J. Geophys. Res., 86*, 8941–8956.

Birn J., M. Hesse, and K. Schindler (2006a), On the role of entropy conservation and entropy loss governing substorm phases, *Int. Conf. Substorms-8*, 19–24.

Birn J., M. Hesse, and K. Schindler (2006b), Entropy conservation in simulations of magnetic reconnection, *Phys. Plasmas, 13,* 092117, DOI:10.1063/1.2349440.

Birn, J., M. Hesse, K. Schindler, and S. Zaharia (2009), Role of entropy in magnetotail dynamics, *J. Geophys. Res., 114*, A00D03, doi:10.1029/2008JA014015.

Birn, J., R. Nakamura, E. V. Panov, and M. Hesse (2011), Bursty bulk flows and dipolarization in MHD simulations of magnetotail reconnection, *J. Geophys. Res., 116*, A01210, doi:10.1029/2010JA016083.

Bouhram, M., B. Klecker, G. Paschmann, S. Haaland, H. Hasegawa, H. Reme, J.-A. Sauvaud, L. M. Kistler, and A. Balogh (2005), Survey of energetic O^+ near the dayside mid-latitude megnetopause with Cluster, *Ann. Geophys., 23*, 1281 - 1294.

Borovsky, J. E., R. C. Elphic, H. O. Funsten, and M. F. Thomsen (1997), The Earth's plasma sheet as a laboratory for turbulence in high-beta MHD, *J. Plasma Phys., 57,* 1 – 34.

Borovsky, J. E., M. F. Thomsen, and R. C. Elphic (1998a), The driving of the plasma sheet by the solar wind, *J. Geophys. Res., 103,* 17, 617–17,639.

Borovsky, J. E., M. F. Thomsen, R. C. Elphic, T. E. Cayton, and D. J. McComas (1998b), The transport of plasma sheet material from the distant tail to geosynchronous orbit, *J. Geophys. Res., 103*, A9, 20,297–20,331.

Borovsky, J. E., and H. O. Funsten (2003), MHD turbulence in the Earth's plasma sheet: Dynamics, dissipation, and driving, *J. Geophys. Res., 108*, 1284, doi:10.1029/2002JA009625.

Brambles, O. J., W. Lotko, P. A. Damiano, B. Zhang, M. Wiltberger, and J. Lyon (2010), Effects of causally driven cusp O+ outflow on the storm time magnetosphere-ionosphere system using a multifluid global simulation, *J. Geophys. Res., 115,* A00J04, doi:10.1029/2010JA015469.

Bristow, W. (2008), Statistics of velocity fluctuations observed by SuperDARN under steady interplanetary magnetic field conditions, *J. Geophys. Res., 113*, A11202, doi:10.1029/2008JA013203.

Burch, J. L., Goldstein, J., Hill, T. W., Young, D. T., Crary, F. J., Coates, A. J., Andre, N., Kurth, W. S., Sittler Jr., E. C. (2005), Properties of local plasma injections in Saturn's magnetosphere, *Geophys. Res. Lett., 32*(14), L14S02.

Chappell, C. R., T. E. Moore, and J. H. Waite Jr. (1987), The ionosphere as a fully adequate source of plasma for the Earth's magnetosphere, J. *Geophys. Res., 92*(A6), 5896 – 5910, doi:10.1029/JA092iA06p05896.

Chaston, C. C., T. D. Phan, J. W. Bonnell, F. S. Mozer, M. Acun, M. L. Goldstein, A. Balogh, M. Andre, H. Reme, and A. Fazakerley (2005), Drift-Kinetic Alfven Waves Observed near a Reconnection X Line in the Earth's Magnetopause, *Phys. Rev. Lett., 95*(6), 065002.

Chaston, C. C., M. Wilber, F. S. Mozer, M. Fujimoto, M. L. Goldstein, M. Acuna, M. H. Reme, and A. Fazakerley (2007), Mode Conversion and Anomalous Transport in Kelvin-Helmholtz Vortices and Kinetic Alfven Waves at the Earth's Magnetopause, *Phys. Rev. Lett., 99*, 175004.

Chaston, C., et al. (2008), Turbulent heating and cross-field transport near the magnetopause from THEMIS, *Geophys. Res. Lett., 35*, L17S08, doi:10.1029/2008GL033601.

Chaston, C.C., J.R. Johnson, M. Wilber, M. Acuna, M.L. Goldstein, and H. Reme (2009), Kinetic Alfven Wave Turbulence and Transport through a Reconnection Diffusion Region, *Phys. Rev. Lett., 102*, 015001.

Chen, C. X., and R. A. Wolf (1993), Interpretation of high-speed flows in the plasma sheet, *J. Geophys. Res., 98*, 21,409-21,419.

Chen, C. X., and R. A. Wolf (1999), Theory of think-filament motion in Earth's magnetotail and its application to bursty bulk flows, *J. Geophys. Res., 104*(A7), 14,613 – 14,626, doi:10.1029/1999A900005.

Chen, L. (1999), Theory of plasma transport induced by low-frequency hydromagnetic waves, *J. Geophys. Res., 104*(A2), 2421–2427, doi:10.1029/1998JA900051.

Crooker, N. U. (1979), Dayside merging and cusp geometry, *J. Geophys. Res., 84*(A3), 951–959, doi:10.1029/JA084iA03p00951.

Collin, H. L., W. K. Peterson, J. F. Drake, and A. W. Yau (1988), The helium components of energetic terrestrial ion upflows: Their occurrence, morphology, and intensity, *J. Geophys. Res., 93*, 7558–7564, doi:10.1029/JA093iA07p07558.

Denton, M. H., M. F. Thomsen, H. Korth, S. Lynch, J. C. Zhang, and M. W. Liemohn (2005), Bulk plasma properties at geosynchronous orbit, *J. Geophys. Res., 110*, A07223, doi:10.1029/2004JA010861.

Delamere, P. A., R. J. Wilson, and A. Masters (2011), Kelvin-Helmholtz instability at Saturn's magnetopause: Hybrid simulations, *J. Geophys. Res., 116*, A10222, doi:10.1029/2011JA016724.

Dubyagin, S., V. Sergeev, S. Apatenkov, V. Angelopoulos, A. Runov, R. Nakamura, W. Baumjohann, J. McFadden, and D. Larson (2011), Can flow bursts penetrate into the inner magnetosphere? *Geophys. Res. Lett., 38*, L08102, doi:10.1029/2011GL047016.

Dungey, J. W. (1961), Interplanetary magnetic field and the auroral zone, *Phys. Res. Lett., 6*, 47.

Erickson, G. M. and R. A. Wolf (1980), Is steady convection possible in the Earth's magnetotail?. *Geophysical Research Letters, 7*: 897–900. doi: 10.1029/GL007i011p00897.

Fairfield, D. H., A. Otto, T. Mukai, S. Kokubun, R. P. Lepping, J. T. Steinberg, A. J. Lazarus, and T. Yamamoto (2000), Geotail observations of the Kelvin-Helmholtz instability at the equatorial magnetotail boundary for parallel northward fields, *J. Geophys. Res., 105*, 21,159-21,173.

Friedel, R. H. W., H. Korth, M. G. Henderson, M. F. Thomsen, and J. D. Scudder (2001), Plasma sheet access to the inner magnetosphere, *J. Geophys. Res., 106*(A4), 5845–5858, doi:10.1029/2000JA003011.

Fujimoto, M., and T. Terasawa (1994), Anomalous ion mixing within an MHD scale Kelvin-Helmholtz vortex, *J. Geophys. Res., 99*, 8601-8614.

Fujimoto, M., and T. Terasawa (1995), Anomalous ion mixing within an MHD scale Kelvin-Helmholtz vortex, 2, Effects of inhomogeneity, *J. Geophys. Res., 100*, 12,025-12,034.

Fujimoto, M., T. Terasawa, T. Mukai, Y. Saito, T. Yamamoto, and S. Kokubun (1998), Plasma entry from the flanks of the near-Earth magnetotail: Geotail observations, *J. Geophys. Res., 103*(A3), 4391–4408, doi:10.1029/97JA03340.

Fujimoto, M., T. Tonooka, and T. Mukai (2003), Vortex-like fluctuations in the magnetotail flanks and their possible roles in plasma transport, in *Earth's Low-Latitude Boundary Layer*, edited by P. Newell, and T. Onsager, Geophysical Monograph, pp. 241-251, AGU.

Fuselier, S. A., J. Berchem, K. J. Trattner, and R. Friedel (2002), Tracing ions in the cusp and low-latitude boundary layer using multispacecraft observations and a global MHD simulation, *J. Geophys. Res., 107*, A9, 1226, doi:10.1029/2001JA000130.

Garner, T. W., R. A. Wolf, R. W. Spiro, M. F. Thomsen, and H. Korth (2003), Pressure balance inconsistency exhibited in a statistical model of magnetospheric plasma, *J. Geophys. Res., 108*, 1331, doi:10.1029/2003JA009877.

Garcia, K. S., V. G. Merkin, and W. J. Hughes (2010), Effects of nightside O+ outflow on magnetospheric dynamics: Results of multifluid MHD modeling, *J. Geophys. Res., 115*, A00J09, doi:10.1029/2010JA015730.

Gold, T. (1959), Motions in the magnetosphere of the earth, *J. Geophys. Res., 64*, 1219.

Guild, T. B., H. E. Spence, E. L. Kepko, V. Merkin, J. G. Lyon, M. Wiltberger, and C. C. Goodrich (2008), Geotail and LFM comparisons of plasma sheet climatology: 1. Average values, *J. Geophys. Res., 113*, A04216, doi:10.1029/2007JA012611.

Guo, X. C., C. Wang, and Y. Q. Hu (2010), Global MHD simulation of the Kelvin-Helmholtz instability at the magnetopause for northward interplanetary magnetic field, *J. Geophys. Res., 115*, A10218, doi:10.1029/2009JA015193.

Hasegawa, A., and L. Chen (1975), Kinetic process of the plasma heating by Alfven wave, *Phys. Rev. Lett., 35*, 370.

Hasegawa, A., and K. Mima (1978), Anomalous transport produce by kinetic alfven wave turbulence, *J. Geophys. Res., 83*, 1117.

Hasegawa, H., M. Fujimoto, K. Maezawa, Y. Saito, and T. Mukai (2003), Geotail observations of the dayside outer boundary region: Interplanetary magnetic field control and dawn-dusk asymmetry, *J. Geophys. Res., 108* (A4), 1163, doi:1029/2002JA009667.

Hasegawa, H., M. Fujimoto, Y. Saito, and T. Mukai (2004a), Dense and stagnant ions in the low-latitude boundary region under northward interplanetary magnetic field, *Geophys. Res. Lett., 31*, L06802, doi:10.1029/2003GL19120.

Hasegawa, H., M. Fujimoto, T.-D. Phan, H. Rème, A. Balogh, M. W. Dunlop, C. Hashimoto, and R. TanDokoro (2004b), Transport of solar wind into Earth's magnetosphere through rolled-up Kelvin-Helmholtz vortices, *Nature, 430*, 755-758.

Hasegawa, H., M. Fujimoto, K. Takagi, Y. Saito, T. Mukai, and H. Rème (2006), Single-spacecraft detection of rolled-up Kelvin-Helmholtz vortices at the flank magnetopause, *J. Geophys. Res., 111*, A09203, doi:10.1029/2006JA011728.

Hill, T. W. (1976), Interchange stability of a rapidly rotating magnetosphere, *Planet. Space Sci., 24*, 1151.

Hill, T. W., et al. (2005), Evidence for rotationally driven plasma transport in Saturn's magnetosphere, *Geophys. Res. Lett., 32*, L14S10.

Hwang, K.-J., M. M. Kuznetsova, F. Sahraoui, M. L. Goldstein, E. Lee, and G. K. Parks (2011), Kelvin-Helmholtz waves under southward interplanetary magnetic field, *J. Geophys. Res., 116*, A08210, doi:10.1029/2011JA016596.

Johnson, J. R., and C. Z. Cheng (1997), Kinetic Alfven waves and plasma transport at the magnetopause, *Geophys. Res. Lett., 24*, 1423-1426.

Johnson, J. R., and C. Z. Cheng (2001), Stochastic ion heating at the magnetopause due to kinetic Alfven waves, *Geophys. Res. Lett., 28*, 4421 – 4424.

Johnson, J. R., C. Z. Cheng, and P. Song (2001), Signatures of mode conversion and kinetic Alfven waves at the magnetopause, *Geophys. Res. Lett., 28*(2), 227-230.

Johnson, J. R., and S. Wing (2009), Northward interplanetary magnetic field plasma sheet entropies, *J. Geophys. Res., 114*, A00D08, doi:10.1029/2008JA014017.

Kaufmann, R. L., W. R. Paterson, and L. A. Frank (2004), Pressure, volume, density relationships in the plasma sheet, *J. Geophys. Res., 109*, A08204, doi:10.1029/2003JA010317.

Kaufmann, R. L., W. R. Paterson, and L. A. Frank (2005), Relationships between the ion flow speed, magnetic flux transport rate, and other plasma sheet parameters, *J. Geophys. Res., 110*, A09216, doi:10.1029/2005JA011068.

Kaufmann, R. L., and W. R. Paterson (2008), Ion heat flux and energy transport near the magnetotail neutral sheet, *J. Geophys. Res., 113*, A05207, doi:10.1029/2007JA012929.

Kaufmann, R. L., and W. R. Paterson (2009), Boltzmann H function and entropy in the plasma sheet, *J. Geophys. Res., 114*, A00D04, doi:10.1029/2008JA014030.

Kivelson, M. G., and H. E. Spence (1988), On the possibility of quasistatic convection in the quiet magnetotail, *Geophys. Res., Lett., 15*, 1541-1544.

Korth, H., M. F. Thomsen, J. E. Borovsky, and D. J. McComas (1999), Plasma sheet access to geosynchronous orbit, *J. Geophys. Res., 104*(A11), 25047–25061, doi:10.1029/1999JA900292.

LaBelle, J. , and R. A. Treumann (1988), Plasma waves at the dayside magnetopause, *Space Sci. Rev., 47*, 175.

Lavraud, B., M. F. Thomsen, J. E. Borovsky, M. H. Denton, and T. I. Pulkkinen (2006), Magnetosphere preconditioning under northward IMF: Evidence from the study of coronal mass ejection and corotating interaction region geoeffectiveness, *J. Geophys. Res., 111*, A09208, doi:10.1029/2005JA011566.

Lavraud, B., M. F. Thomsen, S. Wing, M. Fujimoto, M. H. Denton, J. E. Borovsky, A. Aasnes, K. Seki, and J. Weygand (2006),

Observations of two distinct cold, dense ion populations at geosynchronous orbit: local time asymmetry, solar wind dependence and origin, *Ann. Geophys., 24* (12), 3451-3465.

Lavraud, B., et al. (2009), Tracing solar wind plasma entry into the magnetosphere using ion-to-electron temperature ratio, *Geophys. Res. Lett., 36*, L18109, doi:10.1029/2009GL039442.

Le, G., C. T. Russell, J. T. Gosling, and M. F. Thomsen (1996), ISEE observations of low-latitude boundary layer for northward interplanetary magnetic field: Implications for cusp reconnection, *J. Geophys. Res., 101*, 27,239.

Lee, L. C., J. R. Johnson, and Z. W. Ma (1994), Kinetic Alfvén waves as a source of plasma transport at the dayside magnetopause, *J. Geophys. Res., 99*, 17,405-17,411.

Lemon, C., R. A. Wolf, T. W. Hill, S. Sazykin, R. W. Spiro, F. R. Toffoletto, J. Birn, and M. Hesse (2004), Magnetic storm ring current injection modeled with the Rice Convection Model and a self-consistent magnetic field, *Geophys. Res. Lett., 31*, L21801, doi:10.1029/2004GL020914.

Li, W., J. Raeder, J. Dorelli, M. Øieroset, and T. D. Phan (2005), Plasma sheet formation during long period of northward IMF, *Geophys. Res. Lett., 32*, L12S08, doi:10.1029/2004GL021524.

Li, W., J. Raeder, M. F. Thomsen, and B. Lavraud (2008), Solar wind plasma entry into the magnetosphere under northward IMF conditions, *J. Geophys. Res., 113*, A04204, doi:10.1029/2007JA012604.

Li, W., J. Raeder, M. Øieroset, and T. D. Phan (2009), Cold dense magnetopause boundary layer under northward IMF: Results from THEMIS and MHD simulations, J. *Geophys. Res., 114*, A00C15, doi:10.1029/2008JA013497.

Lin Y., Jay R. Johnson, and X. Wang (2012), Three-Dimensional Mode Conversion Associated with Kinetic Alfven Waves, *Phys. Rev. Lett., 109*, 125003, 10.1103/PhysRevLett.109.125003.

Lyons, L. R., et al. (1999), Association between geotail plasma flows and auroral poleward boundary intensifications observed by canopus photometer, *J. Geophys. Res., 104*(A3), 4484 – 4500, doi:10.1029/1998JA900140.

McAndrews, H. J., et al., Plasma in Saturn's nightside magnetosphere and the implications for global circulation, *Plan. Sp. Sci.*, 2009. (includes discussion of Goertz criterion for pinching off of stretched nightside flux tubes -- relevant to tail reconnection injections).

McPherron, R. L., T.-S. Hsu, J. Kissinger, X. Chu, and V. Angelopoulos (2011), Characteristics of plasma flows at the inner edge of the plasma sheet, *J. Geophys. Res., 116*, A00133, doi:10.1029/2010JA015923.

Miura, A.(1995), Dependence of the magnetopause Kelvin-Helmholtz instability on the orientation of the magnetosheath magnetic field, *Geopohys. Res. Lett., 22*, 2993-2996.

Nagata, D., S. Machida, S. Ohtani, Y. Saito, and T. Mukai (2007), Solar wind control of plasma number density in the near-Earth plasma sheet, *J. Geophys. Res., 112*, A09204, doi:10.1029/2007JA012284.

Nakamura, R., W. Baumjohann, M. Brittmacher, V. A. Sergeev, M. Kubyshkina, T. Mukai, and K. Liou (2001), Flow bursts and auroral activations, *J. Geophys. Res., 106*(A6), 10,777 – 10,789.

Nakamura, et al. (2002), Fast flow during current sheet thining, *Geophys. Res. Lett., 29*(23), 2140, doi:10.1029/2002GL016200.

Nakamura, T. K. M., and M. Fujimoto (2005), Magnetic reconnection within rolled-up MHD-scale Kelvin-Helmholtz vortices: Two-fluid simulations including finite electron inertial effects, *Geophys. Res. Lett., 32*, L21102, doi:10.1029/2005GL023362.

Nakamura, R., et al. (2005), Localized fast flow disturbance observed in the plasma sheet and in the ionosphere, *Ann. Geophys., 23*(2), 553 – 566.

Nemecek, Z., J. Safrankova, G. N. Zastenkar, P. Pisoft, and K. I. Paularena (2002), Spa-

tial distribution of the magnetosheath ion flux, *Adv. Space. Res., 30*, 2751 – 2756, doi:10.1016/S0273-1177(02)80402-1.

Nishino, M. N., M. Fujimoto, T. Terasawa, G. Ueno, K. Maezawa, T. Mukai, and Y. Saito (2007), Geotail observations of temperature anisotropy of the two-component protons in the dusk plasma sheet, *Ann. Geophys., 25*, 769 – 777.

Nykyri, K. and A. Otto (2001), Plasma transport at the magnetospheric boundary due to reconnection in Kelvin-Helmholtz vortices, *Geophys. Res. Lett., 28*, 3565-3568.

Nykyri, K. and A. Otto (2004), Influence of the Hall term on KH instability and reconnection inside KH vortices, *Ann. Geophys., 22*, 935 – 949.

Nykyri, K., A. Otto, B. Lavraud, C. Mouikis, L. M. Kistler, A. Balogh, and H. Reme (2006), Cluster observations of reconnection due to the Kelvin-Hemholtz instability at the dawnsdie magnetospheric flank, *Ann. Geophys., 24*, 2619 – 2643.

Ohtani, S., H. J. Singer, and T. Mukai (2006), Effects of the fast plasma sheet flow on the geosynchronous magnetic configuration: Geotail and GOES coordinated study, *J. Geophys. Res., 111*, A01204, doi:10.1029/2005JA011383.

Øieroset, M., J. Raeder, T. D. Phan, S. Wing, J. P. McFadden, W. Li, M. Fujimoto, H. Rème, and A. Balogh (2005), Global cooling and densification of the plasma sheet during an extended period of purely northward IMF on October 22-24, 2003, *Geophys. Res. Lett., 32*, L12S07, doi:10.1029/2004GL021523.

Øieroset, M., T. D. Phan, V. Angelopoulos, J. P. Eastwood, J. McFadden, D. Larson, C. W. Carlson, K.-H. Glassmeier, M. Fujimoto, and J. Raeder (2008), THEMIS multi-spacecraft observations of magnetosheath plasma penetration deep into the dayside low-latitude magnetosphere for northward and strong By IMF, *Geophys. Res. Lett., 35*, L17S11, doi:10.1029/2008GL033661.

Olson, W. P., and K. A. Pfitzer (1985), Magnetospheric responses to the gradient drift entry of solar wind plasma, *J. Geophys. Res., 90*(A11), 10823–10833, doi:10.1029/JA090iA11p10823.

Otto, A., and D. H. Fairfield (2000), Kelvin-Helmholtz instability at the magnetotail boundary: MHD simulation and comparison with Geotail observations, *J. Geophys. Res., 105*, 21,175-21,190.

Paularena, K. I., J. D. Richardson, M. A. Kolpak, C. R. Jackson, and G. L. Siscoe (2001), A dawn-dusk density asymmetry in Earth's magnetosheath, *J. Geophys. Res., 106*(A11), 25377–25394, doi:10.1029/2000JA000177.

Panov, E. V., et al. (2010a), Plasma sheet thickness during a bursty bulk flow reversal, *J. Geophys. Res., 115*, A05213, doi:10.1029/2009JA014743.

Panov, E. V., et al. (2010b), Multiple overshoot and rebound of a bursty bulk flow, *Geophys. Res. Lett., 37*, L08103, doi:10.1029/2009GL041971.

Pedersen, A., C. A. Cattell, C.-G. Fälthammar, K. Knott, P.-A. Lindqvist, R. H. Manka, and F. S. Mozer (1985), Electric fields in the plasma sheet and plasma sheet boundary layer, *J. Geophys. Res., 90*(A2), 1231–1242, doi:10.1029/JA090iA02p01231.

Peterson, W.K., L. Andersson, B. Callahan, S.R. Elkington, R.W. Winglee, J.D. Scudder, H.L. Collin (2009), Geomagnetic activity dependence of O^+ in transit from the ionosphere, *J. Atmos. Solar-Terres. Phys., 71*, 1623-1629, doi:10.1016/j.jastp.2008.11.003.

Peroomian, V., and M. El-Alaoui (2008), The storm-time access of solar wind ions to the nightside ring current and plasma sheet, *J. Geophys. Res., 113*, A06215, doi:10.1029/2007JA012872.

Peroomian, V., M. El-Alaoui, and P. C. Brandt (2011), The ion population of the magnetotail during the 17 April 2002 magnetic storm: Large-scale kinetic simulations and IMAGE/HENA observa-

tions, *J. Geophys. Res., 116*, A05214, doi:10.1029/2010JA016253.

Petrinec, S. M., (2013), On the magnetic field configuration of the magnetosheath, *Terr. Atmos. Ocean. Sci., 24,* 265-272, doi:10.3319/TAO.2012.10.17.02(SEC).

Pontius, D. H.., and R. A. Wolf (1990), Transient flux tubes in the terrestrial magnetoshere, *Geophys. Res. Lett., 17*(1), 49 – 52.

Raeder, J., R. J. Walker, and M. Ashour-Abdalla (1995), The structure of the distant geomagnetic tail during long periods of northward IMF, *Geophys. Res. Lett., 22*, 349.

Raeder et al. (1997), Boundary layer formation in the magnetotail: Geotail observations and comparisons with a global MHD simulation, *Geophys. Res. Lett., 24*, 951.

Redmon, R. J., W. K. Peterson, L. Andersson, and P. G. Richards (2012), Dawnward shift of the dayside O+ outflow distribution: The importance of field line history in O^+ escape from the ionosphere, *J. Geophys. Res., 117*, A12222, doi:10.1029/2012JA018145.

Richard, R. L., R. J. Walker, and M. Ashour-Abdalla (1994), The population of the magnetosphere by solar winds ions when the interplanetary magnetic field is northward. *Geophys. Res. Lett., 21*: 2455–2458. doi: 10.1029/94GL01427.

Rymer, et al. (2009), Cassini evidence for rapid interchange transport at Saturn, *Planet. Space Sci., 57*, 1779-1784.

Sandholt, P. E., C. J. Farrugia, S. W. H. Cowley, W. F. Denig, M. Lester, J. Moen, and B. Lybekk (1999), Capture of magnetosheath plasma by the magnetosphere during northward IMF, *Geophys. Res. Lett., 26*, 2833-2836.

Sanchez, E. R., S. Wing, E. Spanswick, and E. Donovan (2012), Entropy conservation and rate of propagation of bubbles in the Earth's magnetotail: A case study, *J. Geophys. Res., 117*, A05226, doi:10.1029/2011JA017287

Schriver, D., and M. Ashour-Abdalla (1990), Cold plasma heating in the plasma sheet boundary layer: Theory and simulations, *J. Geophys. Res., 95*(A4), 3987–4005, doi:10.1029/JA095iA04p03987.

Schriver, D., M. Ashour-Abdalla, and R. L. Richard (1998), On the origin of the ion-electron temperature difference in the plasma sheet, *J. Geophys. Res., 103*(A7), 14879–14895, doi:10.1029/98JA00017.

Serveev, V. A., V. Angelopoulos, J. T. Gosling, C. A. Cattell, and C. T. Russell (1996), Detection of localized plasma-depleted flux tubes or bubbles in the mid-tail plasma sheet, *J. Geophys. Res., 101*, 10,817 – 10,826, doi:10.1029/96JA00460.

Sergeev, V.A., K. Liou, P. T. Newell, S.-I. Ohtani, M. R. Hairston, and F. Rich (2004), Auroral streamers: Characteristics of associated precipitation, convection and field-aligned currents, *Ann. Geophys., 22*, 537 – 548.

Sergeev, V. A., S. V. Apatenkov, V. Angelopoulos, J. P. McFadden, D. Larson, J. W. Bonnell, M. Kuznetsova, N. Partamies, and F. Honary (2008), Simultaneous THEMIS observations in the near-tail portion of the inner and outer plasma sheet flux tubes at substorm onset, *J. Geophys. Res., 113*, A00C02, doi:10.1029/2008JA013527.

Shay M., and M. Swisdak (2004), Three-Species Collisionless Reconnection: Effect of O^{+} on Magnetotail Reconnection, *Physical Review Letters, 93* 10.1103/PhysRevLett.93.175001.

Sibeck, D. G., et al. (1999), Comprehensive study of the magnetospheric response to a hot flow anomaly, *J. Geophys. Res., 104*(A3), 4577–4593, doi:10.1029/1998JA900021.

Sittler, E. C., Jr., et al. (2005), Preliminary results on Saturn's inner plasmasphere as observed by Cassini: Comparison with Voyager, *Geophys. Res. Lett., 32*, L14S07, doi:10.1029/2005GL022653.

Sittler Jr., E. C., et al. (2006), Cassini observations of Saturn's inner plasmasphere:

Saturn orbit insertion results, *Planet. And Space Sci., 54*, 1197 – 1210.

Slavin, J. A., et al., Simultaneous observations of earthward flow bursts and plasmoid ejection during magnetospheric substorms, *J. Geophys. Res., 107*(A7), doi:10.1029/2000JA003501, 2002.

Stenuit, H., M. Fujimoto, S. A. Fuselier, J.-A. Sauvaud, S. Wing, A. Fedorov, E. Budnik, S. P. Savin, K. J. Trattner, V. Angelopoulos, J. Bonnel, T. D. Phan, T. Mukai, and A. Pedersen (2002), Multi-spacecraft study oin the dynamics of the dusk-flank magnetosphere under northward IMF: January 10-11, 1997, *J. Geophys. Res., 107*(A10), 1333, doi:10.1029/2002JA9009246.

Stepanova, M., V. Pinto, J. A. Valdivia, and E. E. Antonova (2011), Spatial distribution of the eddy diffusion coefficients in the plasma sheet during quiet time and substorms from THEMIS satellite data, *J. Geophys. Res., 116*, A00I24, doi:10.1029/2010JA015887.

Sonnerup, B. U. Ö., and M. J. Laird (1963), On Magnetospheric Interchange Instability, *J. Geophys. Res., 68*(1), 131–139.

Song, P., and C. T. Russell (1992), Model of the formation of the low-latitude boundary layer for strongly northward interplanetary magnetic field, *J. Geophys. Res., 97*, 1411.

Spence, H. E., and M. G. Kivelson (1993), Contributions of the low-latitude boundary layer to the finite width magnetotail convection model, *J. Geophys. Res., 98*(A9), 15487–15496, doi:10.1029/93JA01531.

Taylor, M. G. G. T., and B. Lavraud (2008), Observation of three distinct ion populations at the Kelvin-Helmholtz-unstable magnetopause, *Ann. Geophys., 26*, 1559 – 1566.

Terasawa, T. et al. (1997), Solar wind control of density and temperature in the near-Earth plasma sheet: WIND/GEOTAIL collaboration, *Geophys. Res. Lett., 24*, 935-938.

Thomas, V. A., and D. Winske (1991), Kinetic simulation of the Kelvin-Helmholtz instability at the Venus ionopause, *Geophys. Res. Lett., 18*, 1943-1946.

Thomas, V. A., and D. Winske (1993), Kinetic simulations of the Kelvin-Helmholtz instability at the magnetopause, *J. Geophys. Res., 98*, 11,425-11,438.

Thomsen, M. F., J. E. Borovsky, R. M. Skoug, and C. W. Smith (2003), Delivery of cold, dense plasma sheet material into the near-Earth region, *J. Geophys. Res., 108*, 1151, doi:10.1029/2002JA009544.

Thomsen, M. F., D. B. Reisenfeld, D. M. Delapp, R. L. Tokar, D. T. Young, F. J. Crary, E. C. Sittler, M. A. McGraw, and J. D. Williams (2010), Survey of ion plasma parameters in Saturn's magnetosphere, *J. Geophys. Res., 115*, A10220, doi:10.1029/2010JA015267.

Treumann, R. A., and W. Baumjohann (1988), Particle trapping at a tangential discontinuity: multiple incidence, *Planet. Space Sci., 36*, 1477 – 1484.

Tsurutani, B. T., E. J. Smith, R. R. Anderson, K. W. Ogilvie, J. D. Scudder, D. N. Baker, and S. J. Bame (1982), Lion roars and nonoscillatory drift mirror waves in the magnetosheath, *J. Geophys. Res., 87*, 6060-6072.

Tsyganenko, N. A. (1982), On the convective mechanism for formation of the plasma sheet in the magnetospheric tail, *Planet Space Sci., 30*, 1007-1012.

Tsyganenko, N. A. (1989), A magnetospheric magnetic field model with a warped tail current sheet, *Planet Space Sci., 37*, 5-20.

Tung, Y.-K., C. W. Carlson, J. P. McFadden, D. M. Klumpar, G. K. Parks, W. J. Peria, and K. Liou (2001), Auroral polar cap boundary ion conic outflow observed on FAST, *J. Geophys. Res., 106*(A3), 3603–3614, doi:10.1029/2000JA900115.

Vasyliunas, V. M. (1971), Deep space plasma measurements, in *Methods of Experimental Physics: Plasma Physics, Part B*, vol. 9, edited by R. H. Lovberg and H. R. Griem, pp. 49-88, Academic, Orlando, Fla.

Walsh, B. M., D. G. Sibeck, Y. Wang, and D. H. Fairfield (2012), Dawn-dusk asymmetries in the Earth's magnetosheath, *J. Geophys. Res., 117*, A12211, doi:10.1029/2012JA018240.

Wang, C.-P., L. R. Lyons, M. W. Chen, and R. A. Wolf (2001), Modeling the quiet time inner plasma sheet protons, *J. Geophys. Res., 106*(A4), 6161–6178, doi:10.1029/2000JA000377.

Wang, C.-P., L. R. Lyons, M. W. Chen, and F. R. Toffoletto (2004), Modeling the transition of the inner plasma sheet from weak to enhanced convection, *J. Geophys. Res., 109*, A12202, doi:10.1029/2004JA010591.

Wang, C.-P., L. R. Lyons, J. M. Weygand, T. Nagai, and R. W. McEntire (2006), Equatorial distributions of the plasma sheet ions, their electric and magnetic drifts, and magnetic fields under different interplanetary magnetic field Bz conditions, *J. Geophys. Res., 111*, A04215, doi:10.1029/2005JA011545.

Wang, C.-P., L. R. Lyons, T. Nagai, J. M. Weygand, and R. W. McEntire (2007), Sources, transport, and distributions of plasma sheet ions and electrons and dependences on interplanetary parameters under northward interplanetary magnetic field, *J. Geophys. Res., 112*, A10224, doi:10.1029/2007JA012522.

Wang, C.-P., L. R. Lyons, R. A. Wolf, T. Nagai, J. M. Weygand, and A. T. Y. Lui (2009), Plasma sheet P5/3 and n and associated plasma and energy transport for different convection strengths and AE levels, *J. Geophys. Res., 114*, A00D02, doi:10.1029/2008JA013849.

Wang, C.-P., L. R. Lyons, T. Nagai, J. M. Weygand, and A. T. Y. Lui (2010), Evolution of plasma sheet particle content under different interplanetary magnetic field conditions, *J. Geophys. Res., 115*, A06210, doi:10.1029/2009JA015028.

Wang, C.-P., M. Gkioulidou, L. R. Lyons, and V. Angelopoulos (2012), Spatial distributions of the ion to electron temperature ratio in the magnetosheath and plasma sheet, *J. Geophys. Res., 117*, A08215, doi:10.1029/2012JA017658.

Weygand, J. M., et al. (2005), Plasma sheet turbulence observed by Cluster II, *J. Geophys. Res., 110*, A01205, doi:10.1029/2004JA010581.

Wilber, M., and R. M. Winglee (1995), Dawn-dusk asymmetries in the low-latitude boundary layer arising from the Kelvin-Helmholtz instability: A particle simulation, *J. Geopshys. Res., 100*, 1883-1898.

Wilson, G. R., D. M. Ober, G. A. Germany, and E. J. Lund (2001), The relationship between suprathermal heavy ion outflow and auroral electron energy deposition: Polar/Ultraviolet Imager and Fast Auroral Snapshot/Time-of-Flight Energy Angle Mass Spectrometer observations, *J. Geophys. Res., 106*(A9), 18981–18993, doi:10.1029/2000JA000434.

Wiltberger, M., W. Lotko, J. G. Lyon, P. Damiano, and V. Merkin (2010), Influence of cusp O+ outflow on magnetotail dynamics in a multifluid MHD model of the magnetosphere, *J. Geophys. Res., 115*, A00J05, doi:10.1029/2010JA015579.

Winske, D., and N. Omidi (1995), Diffusion at the magnetopause: Hybrid simulations, *J. Geophys. Res., 100*(A7), 11923–11933, doi:10.1029/94JA02730.

Wing, S. and P. T. Newell (1998), Central plasma sheet ion properties as inferred from ionospheric observations, *J. Geophys. Res., 103*, 6785-6800.

Wing, S., and P. T. Newell (2002), 2D plasma sheet ion density and temperature profiles for northward and southward IMF, *Geophys. Res. Lett., 29*, doi:10.1029/2001GL013950.

Wing, S., J. R. Johnson, P. T. Newell, and C.-I. Meng (2005), Dawn-dusk asymmetries, ion spectra, and sources in the northward interplanetary magnetic field plasma sheet, *J. Geophys. Res., 110*, A08205, doi:10.1029/2005JA011086.

Wing, S., J. R. Johnson, and M. Fujimoto (2006), Timescale for the formation of the cold-dense plasma sheet: A case study,

Geophys. Res. Lett., 33, L23106, doi:10.1029/2006GL027110.

Wing, S., J. W. Gjerloev, J. R. Johnson, and R. A. Hoffman (2007), Substorm plasma sheet ion pressure profiles, *Geophys. Res. Lett., 34*, L16110, doi:10.1029/2007GL030453.

Wing, S., and J. R. Johnson (2009), Substorm entropies, *J. Geophys. Res., 114*, A00D07, doi:10.1029/2008JA013989.

Wing, S., and J. R. Johnson (2010), Introduction to special section on Entropy Properties and Constraints Related to Space Plasma Transport, *J. Geophys. Res., 115*, A00D00, doi:10.1029/2009JA014911.

Wing, S., M. Gkioulidou, J. R. Johnson, P. T. Newell, and C.-P. Wang (2013), Auroral particle precipitation characterized by the substorm cycle, *J. Geophys. Res. Space Physics, 118*, 1022–1039, doi:10.1002/jgra.50160.

Winglee, R. M., D. Chua, M. Brittnacher, G. K. Parks, and G. Lu (2002), Global impact of ionospheric outflows on the dynamics of the magnetosphere and cross-polar cap potential, *J. Geophys. Res., 107*(A9), 1237, doi:10.1029/2001JA000214.

Winglee, R. M., W. Lewis, and G. Lu (2005), Mapping of the heavy ion outflows as seen by IMAGE and multifluid global modeling for the 17 April 2002 storm, *J. Geophys. Res., 110*, A12S24, doi:10.1029/2004JA010909.

Wolf, R. A., V. Kumar, F. R. Toffoletto, G. M. Erickson, A. M. Savoie, C. X. Chen, and C. L. Lemon (2006), Estimating local plasma sheet PV5/3 from single-spacecraft measurements, *J. Geophys. Res., 111*, A12218, doi:10.1029/2006JA012010.

Wolf, R. A., Wan, X. Xing, J. Zhang, and S. Sazykin (2009), Entropy and plasma sheet transport, *J. Geophys. Res., 114*, A00D05, doi:10.1029/2009JA014044.

Wolf, R. A., C. X. Chen, and F. R. Toffoletto (2012), Thin filament simulations for Earth's plasma sheet: Interchange oscillations, *J. Geophys. Res., 117*, A02215, doi:10.1029/2011JA016971.

Yao, Y., C. C. Chaston, K.-H. Glassmeier, and V. Angelopoulos (2011), Electromagnetic waves on ion gyro-radii scales across the magne- topause, *Geophys. Res. Lett., 38*, L09102, doi:10.1029/2011GL047328.

Young et al. (2005), Composition and Dynamics of Plasma in Saturn's Magnetosphere, *Science*, 307, 1262.

Zhang, J.-C., R. A. Wolf, S. Sazykin, and F. R. Toffoletto (2008), Injection of a bubble into the inner magnetosphere, *Geophys. Res. Lett., 35*, L02110, doi:10.1029/2007GL032048.

Zhou, X.-Z., Z. Y. Pu, Q.-G. Zong, and L. Xie (2007), Energy filter effect for solar wind particle entry to the plasma sheet via flank regions during southward interplanetary magnetic field, *J. Geophys. Res., 112*, A06233, doi:10.1029/2006JA012180.